









# Daylength variation affects growth, photosynthesis, leaf metabolism, partitioning, and metabolic fluxes

Yuan Xu <sup>1,2</sup> Abubakarr A. Koroma <sup>1,3</sup> Sean E. Weise <sup>2,4</sup> Xinyu Fu <sup>2</sup> Thomas D. Sharkey <sup>2,4,5,\*</sup> and Yair Shachar-Hill <sup>1,\*</sup>

- 1 Department of Plant Biology, Michigan State University, East Lansing, MI 48824, USA
- 2 MSU-DOE Plant Research Laboratory, Michigan State University, East Lansing, MI 48824, USA
- 3 Department of Microbiology and Immunology, Emory University, Atlanta, GA 30329, USA
- 4 Department of Biochemistry and Molecular Biology, Michigan State University, East Lansing, MI 48824, USA
- 5 Plant Resilience Institute, Michigan State University, East Lansing, MI 48824, USA

\*Author for correspondence: tsharkey@msu.edu (T.D.S.), yairhill@msu.edu (Y.S.-H.)

The author responsible for distribution of materials integral to the findings presented in this article in accordance with the policy described in the Instructions for Authors (<https://academic.oup.com/plphys/pages/General-Instructions>) is Thomas D. Sharkey.

## Abstract

Daylength, a seasonal and latitudinal variable, exerts a substantial impact on plant growth. However, the relationship between daylength and growth is nonproportional, suggesting the existence of adaptive mechanisms. Thus, our study aimed to comprehensively investigate the adaptive strategies employed by plants in response to daylength variation. We grew false flax (*Camelina sativa*) plants, a model oilseed crop, under long-day (LD) and short-day (SD) conditions and used growth measurements, gas exchange measurements, and isotopic labeling techniques, including <sup>13</sup>C, <sup>14</sup>C, and <sup>2</sup>H<sub>2</sub>O, to determine responses to different daylengths. Our findings revealed that daylength influences various growth parameters, photosynthetic physiology, carbon partitioning, metabolic fluxes, and metabolite levels. SD plants employed diverse mechanisms to compensate for reduced CO<sub>2</sub> fixation in the shorter photoperiod. These mechanisms included enhanced photosynthetic rates and reduced respiration in the light ( $R_L$ ), leading to increased shoot investment. Additionally, SD plants exhibited reduced rates of the glucose 6-phosphate (G6P) shunt and greater partitioning of sugars into starch, thereby sustaining carbon availability during the longer night. Isotopic labeling results further demonstrated substantial alterations in the partitioning of amino acids and TCA cycle intermediates between rapidly and slowly turning over pools. Overall, the results point to multiple developmental, physiological, and metabolic ways in which plants adapt to different daylengths to maintain growth.

## Introduction

Daylength or photoperiod varies with the season and latitude and strongly influences plant growth (Casal et al. 2004; Jackson 2009). However, the relationship between daylength and growth is not proportional, as shorter days result in reduced growth that is not directly proportional to the duration of the day. This indicates the presence of adaptive mechanisms. Therefore, the goal of this study was to quantify comprehensively the ways in which a model plant adapts to daylength.

False flax (*Camelina sativa*), a model C<sub>3</sub> crop plant, presents an intriguing study system as a temperate annual cultivated across diverse latitudes and during distinct seasons, such as spring and winter, which exhibit varying daylengths (Righini et al. 2019; Kurasiak-Popowska et al. 2021). Genetic and other resources have been developed in recent years for this species, which is a close relative of *Arabidopsis* (*Arabidopsis thaliana*) (Gomez-Cano et al. 2020). *Camelina* has recently gained increased attention because of the rising demand for biofuel (Bernardo et al. 2003; Ciubota-Rosie et al.

Received July 14, 2023. Accepted September 01, 2023. Advance access publication September 20, 2023

© The Author(s) 2023. Published by Oxford University Press on behalf of American Society of Plant Biologists.

This is an Open Access article distributed under the terms of the Creative Commons Attribution-NonCommercial-NoDerivs licence (<https://creativecommons.org/licenses/by-nc-nd/4.0/>), which permits non-commercial reproduction and distribution of the work, in any medium, provided the original work is not altered or transformed in any way, and that the work is properly cited. For commercial re-use, please contact [journals.permissions@oup.com](mailto:journals.permissions@oup.com)

Open Access

2013). As an oilseed crop, *Camelina* has high seed oil content suitable for diesel and jet fuel (Shonnard et al. 2010; Berti et al. 2016), potential for widespread application in the food and cosmetic industries (Kurasiak-Popowska et al. 2017), and low cost of production (Budin et al. 1995; Moser and Vaughn 2010) and is highly adaptable to various soil and climate conditions (Zubr 2003). Therefore, a better understanding of *Camelina* grown in different daylength environments is desirable.

Metabolic flux, the flow of metabolites through metabolic pathways and networks, can be assessed by metabolic flux analysis (MFA) by combining extracellular flux measurements and intracellular isotopic labeling measurements (Stephanopoulos et al. 1998; Schwender et al. 2004). Both stable isotopes (e.g.  $^{13}\text{C}$ ,  $^{15}\text{N}$ ,  $^2\text{H}$ , and  $^{18}\text{O}$ ) and radioisotopes (e.g.  $^{14}\text{C}$  or  $^3\text{H}$ ) can be used for isotopic labeling. Steady-state labeling, applied extensively in heterotrophic systems, measures label redistribution after achieving isotopic equilibrium (Guo et al. 2015; Kruger and Ratcliffe 2015; Clark et al. 2020; Li et al. 2022; Sagun et al., 2023). However, it is not suitable for autotrophic systems when labeling becomes evenly distributed among metabolites and atomic positions (Kruger and Ratcliffe 2021). In contrast, dynamic labeling analyzes label redistribution before isotopic equilibrium, making it suitable for autotrophic systems. Recent improvements in  $^{13}\text{CO}_2$  time-course labeling techniques and computational modeling have made isotopically nonstationary MFA (INST-MFA) a powerful tool to study autotrophic carbon metabolism and estimating in vivo carbon fluxes (Shastri and Morgan 2007; Adebiji et al. 2015; Basler et al. 2018; Cheah and Young 2018; Chu et al. 2022).

Metabolic fluxes range over several orders of magnitude, resulting in metabolite turnover times ranging from 10 s of milliseconds for Calvin–Benson cycle (CBC) intermediates to hours for sugars to days for some storage pools. Amino acids, organic acids, and sugars are located in multiple cellular compartments (Gerhardt and Heldt 1984), and their labeling kinetics show multiphasic rates (Xu et al. 2022). While  $^{13}\text{CO}_2$ -labeling probes faster turnover pools, determining turnover rates for low-flux metabolites can be challenging in shorter labeling experiments. Deuterium oxide ( $^2\text{H}_2\text{O}$ ) labeling over longer periods can be used to track slower processes and pools with very slow turnover (Yang et al. 2010). In this study, we utilized both short-term  $^{13}\text{CO}_2$  labeling and long-term  $^2\text{H}_2\text{O}$  labeling to determine the metabolic fluxes of fast pools and the turnover rates and partitioning of slower pools through the network of central metabolism in source leaves. The combination of metabolic flux, pool size, and turnover rate information provides an integrated understanding of plant biochemical responses to varying daylengths.

Our findings demonstrate that short-day (SD) plants employ multiple mechanisms to compensate for reduced  $\text{CO}_2$  fixation due to the shorter photoperiod and consequent reduced daily light integral (DLI) of photons. Firstly, SD plants exhibited a higher photosynthetic rate. Carbon isotope

analysis confirmed a higher  $\text{CO}_2$  concentration at the Rubisco level in SD plants, indicated by greater discrimination. Secondly, SD plants exhibited lower respiration in the light ( $R_L$ ) and reduced flux of the glucose 6-phosphate/oxidative pentose phosphate pathway (G6P/OPPP) shunt, which contributes substantially to  $R_L$ . SD plants potentially enhance photosynthetic efficiency as  $R_L$  is a process that results in carbon loss. Thirdly, SD plants showed a higher rate of starch synthesis, leading to increased starch levels for use during the longer night. Fourthly, SD plants allocated more resources to shoots relative to roots, providing additional resources for photosynthesis. Finally, SD plants had thinner leaves, enabling a larger leaf area with the same resource allocation.

## Results

### Characterization of plant growth, photosynthesis, leaf morphology, and carbon isotope composition

The dry weight (DW) of both shoot and root systems was higher in long-day (LD) plants at all sampling times (Fig. 1A). The higher DW of LD plants at all sampling dates suggested that the daylength effect on growth rate was persistent over time. SD plants have a greater shoot/root ratio (Fig. 1B) and  $\sim 12\%$  less fresh weight per leaf area (Fig. 1C). Leaf chlorophyll content was not affected by different daylength (Supplemental Table S1).

Since mature source leaves provide most of the energy and carbon for plant growth and development, we focused our metabolic and physiological analyses on these tissues. The photosynthetic rate was higher in SD (Table 1). This compensated for the lower DLI. Assuming constant illumination rates over the photoperiod, DLI for the SD was 56% of the LD value. The daily carbon gain calculated from the net carbon fixation rate and daylength (Table 1; Supplemental Table S2) was  $0.86 \text{ mol m}^{-2}$  for LD and  $0.59 \text{ mol m}^{-2}$  for SD or 68% of the carbon gain in LD with just 56% of the photons. Relative growth rate (*rgr*) from Day 14 to Day 28 was  $0.31 \text{ d}^{-1}$  in LD (Table 2). If *rgr* was reduced to 56% of LD ( $0.18 \text{ d}^{-1}$ ) in proportion to the reduced DLI in SD, then a DW of 0.19 g would be expected, compared to the observed 0.74 g (Table 2). Thus, light use efficiency of carbon acquisition was higher in SD than in LD plants. If the increased photosynthetic rate in SD is considered in addition to the decreased DLI, then *rgr* in SD would be expected to be 68% of the *rgr* for LD, i.e.  $0.68 * 0.31 = 0.21 \text{ d}^{-1}$  compared to the observed  $0.27 \text{ d}^{-1}$ , and the final weight would be 0.32 g compared to the observed 0.74 g (Table 2). This suggests that in addition to an increased light use efficiency for carbon acquisition, there is an increased efficiency in the use of carbon for growth.

The higher photosynthetic assimilation rate (*A*) in SD was accompanied by an increase in stomatal conductance (*g*). The increased *g* was just sufficient to keep intercellular  $\text{CO}_2$  ( $C_i$ ) constant. The increased *A* was not the result of increased Rubisco capacity ( $V_{\text{cmax}}$ ) or electron transport (*J*),

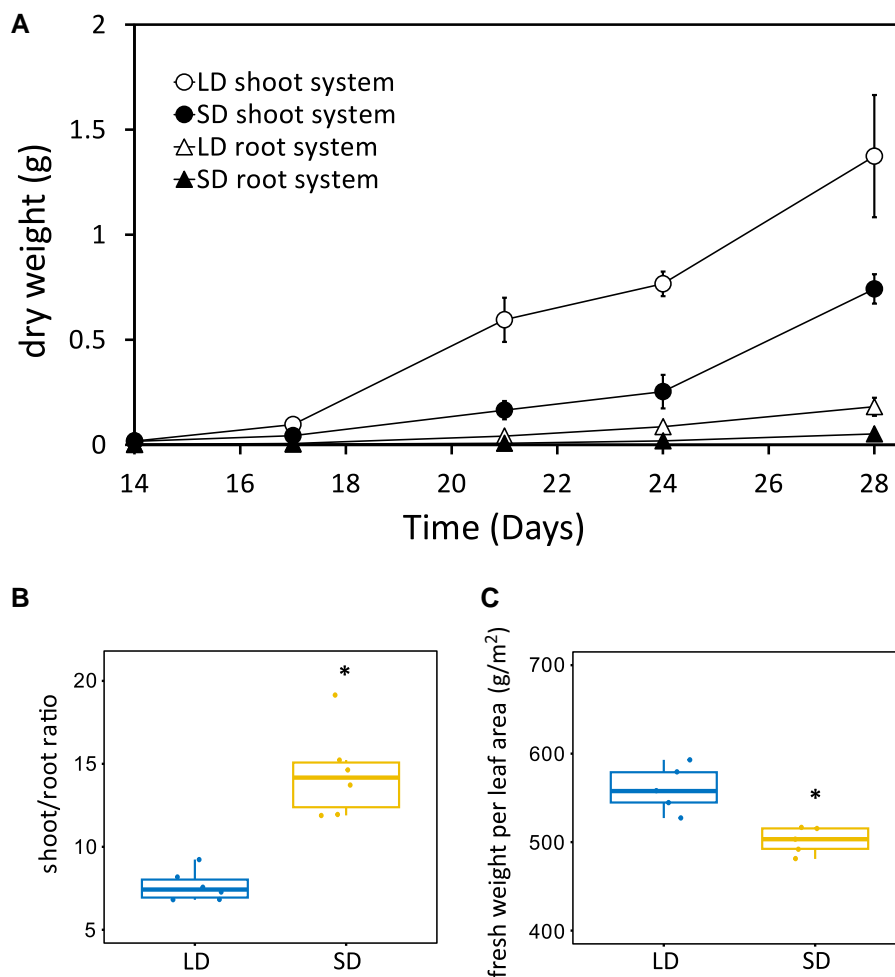


**Figure 1.** The effect of daylength on plant growth and leaf properties. **A)** The DW of the shoot and root system from 14 to 28 d ( $n = 6$ ,  $\pm$ SD). **B)** Shoot/root mass ratio at 28 d ( $n = 6$ ). **C)** Fresh weight per leaf area ( $n = 5$ ). The line in the middle of the boxplots is the median. The bottom and top of the boxplot are at the 25th and 75th percentiles, respectively. The whiskers extend from the boxes and mark the 5th and 95th percentiles. Individual data points are symbolized by circles. Significant differences between LD and SD in **B)** and **C)** are marked with asterisks (Student's  $t$ -test,  $*P \leq 0.05$ ).

**Table 1.** Photosynthesis and  $A/C_i$  curve parameters for LD and SD plants

Parameters	Unit	LD	SD	Significance	
<b>Photosynthesis</b>					
$A$	$\mu\text{mol m}^{-2} \text{s}^{-1}$	$14.9 \pm 0.7$	$18.1 \pm 0.1$	****	10
$g$	$\text{mol m}^{-2} \text{s}^{-1}$	$0.25 \pm 0.03$	$0.31 \pm 0.07$	*	10
$C_i$	$\mu\text{L L}^{-1}$	$282 \pm 15$	$281 \pm 26$	-	10
$\delta^{13}\text{C}$	‰	$-25.1 \pm 0.2$	$-29.9 \pm 0.2$	***	5
<b><math>A/C_i</math> analysis</b>					
$V_{\text{cmax}}$	$\mu\text{mol m}^{-2} \text{s}^{-1}$	$46.1 \pm 5.2$	$46.2 \pm 1.7$	-	4
$J$	$\mu\text{mol m}^{-2} \text{s}^{-1}$	$91.2 \pm 4.6$	$86.3 \pm 4.9$	-	4
$TPU$	$\mu\text{mol m}^{-2} \text{s}^{-1}$	$4.9 \pm 0.6$	$5.3 \pm 0.4$	-	4
$R_L$	$\mu\text{mol m}^{-2} \text{s}^{-1}$	$1.16^a \pm 0.53$	$0.15 \pm 0.17$	*	4
$g_m$	$\mu\text{mol m}^{-2} \text{s}^{-1} \text{Pa}^{-1}$	$14.3 \pm 12.8$	$100^b \pm 0$	-	4
$\alpha_G$	Unitless	$0.02 \pm 0.03$	$0.04 \pm 0.04$	-	4
$\alpha_S$	Unitless	$0.52^a \pm 0.22$	$0.17 \pm 0.09$	*	4

Data are averages  $\pm$  SD. This is a subset of data available in [Supplemental Table S1](#). Significant differences between LD and SD are marked with asterisks (Student's 2-tailed  $t$ -test,  $*P \leq 0.05$ ,  $**P \leq 0.01$ ,  $***P \leq 0.001$ , and  $****P \leq 0.0001$ ).

<sup>a</sup>One outlier sample was not included in the analysis.

<sup>b</sup>The value of 100 is the limit set in the fitting routine and indicates that  $g_m$  was too high to accurately measure.

**Table 2.** Observed and calculated *rgr* and final plant weights

Observed and calculated <i>rgr</i>	<i>rgr</i> (d <sup>-1</sup> )	Weight ( <i>W</i> <sub>2</sub> ) (g)	Weight relative to LD
LD observed	0.31	1.37	1
SD observed	0.27	0.74	0.54
SD A-based adjusted	0.21	0.32	0.23
SD DLI adjusted	0.17	0.19	0.14

The observed DWs for plants in LDs (LD observed) or SDs (SD observed). Multiplying the daylength by assimilation weight for SD/LD gave a value of 0.68 and the LD *rgr* was multiplied by this amount to determine the SD A-based adjusted *rgr*. Assuming the DLI was proportional to daylength the DLI adjusted *rgr* was multiplied by 9/16 or 0.56. The final predicted weight based on adjusted *rgr* was calculated from this equation:

$$W_2 = W_1 \cdot e^{(rgr \cdot (T_2 - T_1))}$$

The value for *W*<sub>1</sub> was 0.02 g for all conditions and *T*<sub>2</sub> - *T*<sub>1</sub> was 14 d. An expanded data sheet and explanation are given in [Supplemental Table S2](#) and [Method S2](#). The alternative analysis resulted in *rgr* values of 0.30 for LD and 0.27 for SD, with corresponding goodness-of-fit *R*<sup>2</sup> values of 0.86 and 0.99 ([Supplemental Table S2](#)).

although respiration in the light (*R*<sub>L</sub>) was reduced, probably contributing to the higher *A* in SD ([Table 1](#)). Mesophyll conductance (*g*<sub>m</sub>) was too high to measure in SD plants but was much less and easily measured in LD plants. The δ<sup>13</sup>C showed much greater discrimination in SD plants. Given the same *C*<sub>i</sub>, this is consistent with a substantially greater *g*<sub>m</sub> in SD plants, which could account for much of the difference in *A*. Labeling with <sup>14</sup>CO<sub>2</sub> showed that an increased proportion of carbon went to starch in SD relative to LD leaves ([Table 3](#)). The fraction of fixed carbon going to sucrose was the same in SD and LD, and the much higher fraction going to starch in SD was at the expense of carbon going to the ionic fraction (amino acids, organic acids, etc.) ([Table 2](#)).

### <sup>13</sup>CO<sub>2</sub> labeling in central metabolism

A <sup>13</sup>CO<sub>2</sub>-labeling experiment was performed at 10 time points with 43 fragment ions analyzed by liquid chromatography–tandem mass spectrometry (LC-MS/MS) and gas chromatography–mass spectrometry (GC-MS) ([Supplemental Table S3](#)). Most metabolites showed a consistent increase of <sup>13</sup>C enrichment over time ([Fig. 2](#); [Supplemental Table S4](#)) and a gradual transition of mass isotopolog distributions (MIDs) to heavier isotopologs over time ([Supplemental Figs. S1 and S2](#) and [Table S3](#)). The fitted labeling kinetics for most metabolites align with the measured MIDs ([Supplemental Figs. S1 and S2](#)). Metabolites showed very different labeling kinetics that reflect network proximity and pathway activity. All CBC intermediates showed fast labeling ([Fig. 2A](#); [Supplemental Fig. S2A](#)) that is consistent with their short half-times ([Arrivault et al. 2009](#); [Hasunuma et al. 2010](#); [Szecowka et al. 2013](#); [Ma et al. 2014](#)). The TCA cycle intermediates showed limited labeling over 30 min ([Fig. 2A](#); [Supplemental Fig. S2B](#)), which is consistent with previous findings in *Arabidopsis* ([Arrivault et al. 2009](#); [Szecowka et al. 2013](#); [Ma et al. 2014](#)), *Camelina* ([Xu et al. 2021, 2022](#)), and tobacco (*Nicotiana tabacum*) ([Fu et al. 2022](#)). The limited fractional labeling of TCA intermediates may be caused by large inactive vacuolar pools that dilute the label in these metabolites and by low fluxes

**Table 3.** Fractions of starch and sucrose measured by <sup>14</sup>C radioactivity in LD and SD (*n* = 6, ±sd)

Fractions of starch and sucrose	LD	SD
Total soluble (kBq g <sup>-1</sup> FW)	12.6 ± 0.6	17.1 ± 2.1*
Starch (kBq g <sup>-1</sup> FW)	4.0 ± 0.3	8.9 ± 1.7*
Neutral soluble (kBq g <sup>-1</sup> FW)	7.6 ± 0.8	12.2 ± 1.9*
Ionic fraction (kBq g <sup>-1</sup> FW)	5.0 ± 0.5	4.8 ± 0.9
Starch/total	0.24 ± 0.02	0.34 ± 0.03*
Sucrose/total	0.46 ± 0.03	0.47 ± 0.05
Ionic/total	0.30 ± 0.04	0.19 ± 0.03*
Starch (μmol m <sup>-2</sup> s <sup>-1</sup> )	3.4 ± 0.3	6.1 ± 0.5*
Sucrose (μmol m <sup>-2</sup> s <sup>-1</sup> )	6.8 ± 0.4	8.5 ± 0.9*

Significant differences between LD and SD are marked with asterisks (Student's 2-tailed *t*-test, *P* ≤ 0.05).

through active cytosolic and mitochondrial pools during photosynthesis. Other metabolites showed intermediate rates of labeling ([Fig. 2A](#); [Supplemental Table S4](#)).

The <sup>13</sup>C fractional labeling of glycine, serine, and alanine was slower and reached lower levels in leaves in SD ([Fig. 2B](#); [Supplemental Fig. S1](#) and [Table S4](#)). In leaves of LD plants, glycine showed rapid labeling with high <sup>13</sup>C enrichment at 30 min (87%) that was comparable to labeling in CBC intermediates but showed much slower and lower labeling in SD leaves (30%, [Fig. 2B](#); [Supplemental Table S4](#)). Serine and alanine were labeled to 81% and 57%, respectively, after 30 min in LD leaves, but only to 73% and 40%, respectively, in SD leaves ([Fig. 2B](#); [Supplemental Table S4](#)).

In contrast, the <sup>13</sup>C label incorporation into glycerate, aspartate, threonine, and sucrose was faster and higher in the leaves of SD plants ([Fig. 2B](#); [Supplemental Fig. S1](#) and [Table S4](#)). At 30 min, glycerate, aspartate, sucrose glucosyl moiety, and sucrose fructosyl moiety were labeled to between 39% and 54% in SD but only 17% to 35% in LD ([Fig. 2B](#); [Supplemental Table S4](#)).

### Metabolic fluxes of central metabolism

With a comprehensive, model-based analysis of isotopic labeling dynamics, INST-MFA provided a global assessment of flux differences between LD and SD plants. Because isotopically labeled CO<sub>2</sub> results in uninformative uniformly labeled products, we use INST-MFA over steady-state MFA for quantifying leaf metabolic fluxes ([Young et al. 2011](#)). In addition, while the plants are actively growing during the experimental period ([Fig. 1](#)), with roots and younger leaves and shoots being sink tissues, the mature source leaves whose metabolic fluxes were analyzed are no longer growing. Turnover of biomass components in mature leaves is very slow compared to carbon assimilation rates. For example, lipid turnover rates are estimated to involve carbon fluxes over 1,000 times lower than photosynthetic rates (as discussed in [Xu et al. 2021](#)), and cell wall turnover is considerably slower. Therefore, unlike MFA applied to growing tissues, the biomass composition was not necessary for flux mapping. Metabolic fluxes were estimated from the short-term labeling data and the measured rates of starch accumulation, CO<sub>2</sub> fixation, and the proportions of metabolites exported.



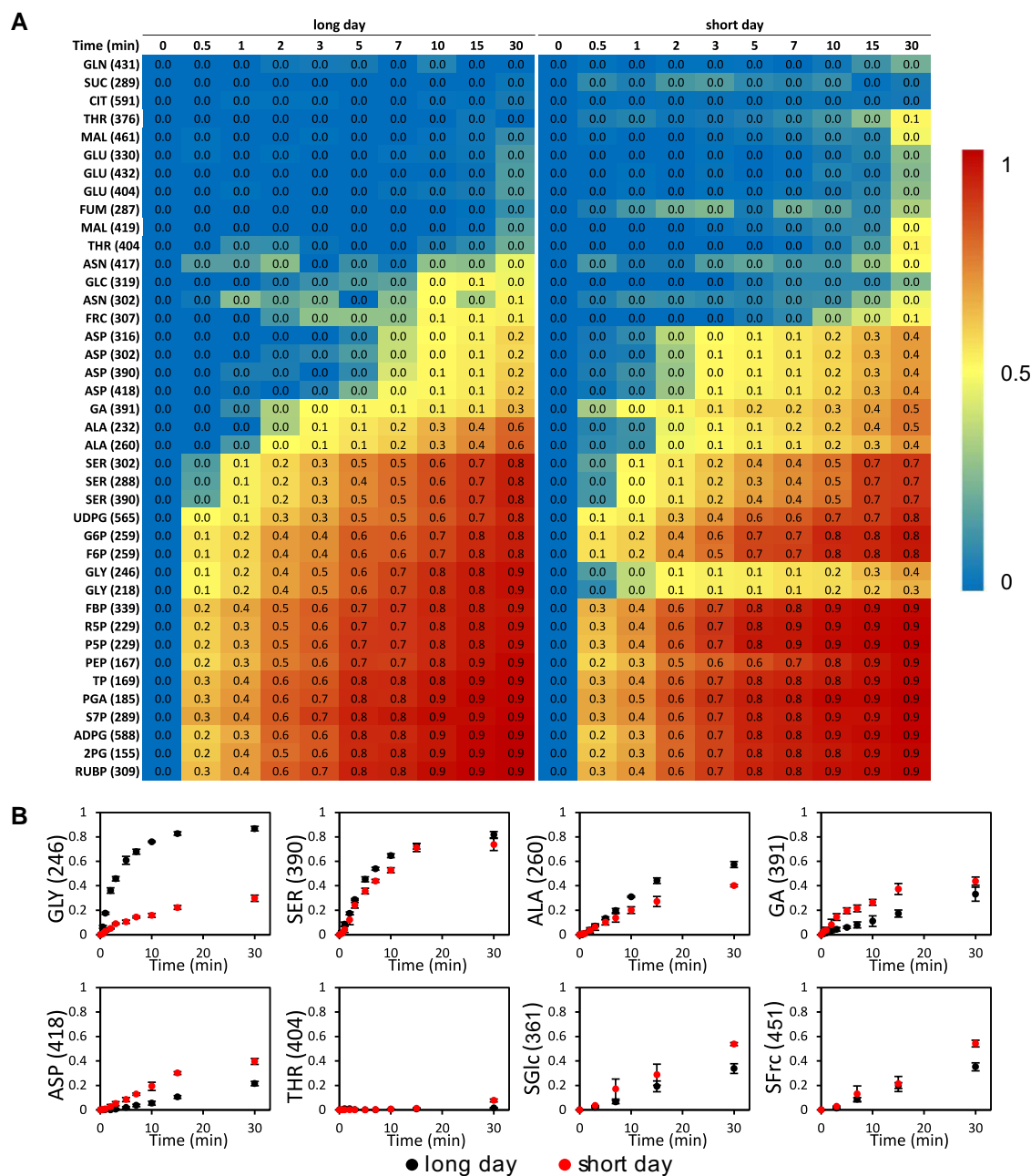


**Figure 2.**  $^{13}\text{C}$  enrichment of measured metabolites in LD and SD conditions. **A)** Heatmap of  $^{13}\text{C}$  enrichment of metabolites from 0 to 30 min. The gradient bar represented the value of  $^{13}\text{C}$  enrichment from low to high. **B)**  $^{13}\text{C}$  enrichment ( $n = 3$ ,  $\pm\text{sd}$ ) of glycine, serine, alanine, glycerate, aspartate, threonine, sucrose glucosyl moiety (SGlc), and sucrose fructosyl (SFrc) moiety from 0 to 30 min. The x axis represents the time of labeling (in minutes), while the y axis represents the fraction of  $^{13}\text{C}$  enrichment.

INST-MFA was conducted using these data and a reaction network model developed previously (Xu et al. 2022) that integrates the CBC, photorespiration, the TCA cycle, a G6P/OPPP shunt, cytosolic and vacuolar sugar pools, and biosynthesis pathways for starch, sucrose, and amino acids (Xu et al. 2022). The sum-of-squared residuals (SSRs) between measured and simulated data for LD and SD models are 825 and 647, respectively, which were both accepted by the  $\chi^2$  goodness of fit test. Absolute fluxes obtained from the best-fit values were normalized to the measured net assimilation

rate to enable comparisons of the distribution of photosynthate between leaves of LD and SD plants (Supplemental Table S5). The 95% confidence intervals for both absolute and normalized fluxes were estimated by the parameter continuation method (Supplemental Table S5).

Both the absolute and normalized flux through the G6P/OPPP shunt were higher in LD plants, as were the normalized fluxes of plastid triose phosphate to cytosolic triose phosphate and cytosolic hexose phosphate synthesis (Fig. 3A; Supplemental Table S5). This carbon recycling pathway

from chloroplast to cytosol as triose phosphate and back to the chloroplast as pentose phosphate carried a substantially higher flux in LD plants. The normalized flux for glutamate synthesis via the TCA cycle was higher in LD plants (Fig. 3A; Supplemental Table S5). The nonphotorespiratory CO<sub>2</sub> release estimated by INST-MFA from the sum of all non-photorespiratory CO<sub>2</sub> releasing reactions was higher in LD plants (Supplemental Table S5), which is consistent with higher  $R_L$  value measured by gas exchange (Table 1).

SD plants showed higher overall absolute fluxes through CBC and photorespiratory intermediates (Fig. 3B). However, after normalization to the net CO<sub>2</sub> assimilation rate, the fluxes were comparable between LD and SD plants (Supplemental Table S5), indicating the differences were mainly caused by the higher net CO<sub>2</sub> assimilation rate. Both the absolute and normalized fluxes for starch and alanine synthesis were higher in SD plants (Fig. 3B; Supplemental Table S5), indicating the preferential carbon partitioning to starch and alanine in SD plants.

The export fluxes of sucrose to vascular exudate were comparable between LD and SD plants (Fig. 3, A and B; Supplemental Table S5). Alanine, glycine, and serine had higher export fluxes in SD plants (Supplemental Table S6). Glutamate and aspartate had similar export fluxes in plants grown at different daylengths (Supplemental Table S6).

### **<sup>2</sup>H labeling of metabolites with slower turnover rates**

Because TCA cycle intermediates and most free amino acids showed less than 6% total <sup>13</sup>C enrichment over 30 min under both daylength conditions (Fig. 2A; Supplemental Fig. S2B and Table S4), longer labeling times were used to monitor the turnover kinetics of these metabolites with deuterium oxide as tracer. Labeling of organic acids and amino acids was measurable within 9 h (Fig. 4) and for the amino acids followed monoexponential kinetics with a plateau reached within the light period (Supplemental Fig. S3). Succinate, malate, and citrate showed slower turnover in the first 9 h (light period for both LD and SD) and, in the case of citrate and succinate, substantial turnover between 9 and 24 h (Fig. 4B). The <sup>2</sup>H-labeling kinetics for each amino acid were well explained by a model representing an active pool turning over with first-order kinetics and another pool of the same metabolite that did not become substantially labeled during the 9-h daytime labeling period (Supplemental Fig. S3 and Table S7). The relative turnover rates for active pools in LD and SD plants, as well as the relative sizes of the active versus inactive pools, were determined (Supplemental Table S7). We observed that (i) the active pool for all analyzed amino acids and organic acids (except for Asp) represented a higher proportion of the total in LD plants than in SD plants (Supplemental Table S7). The active pools of amino acids showed a narrow range of turnover rates (varying by ±20% for SD and ±25% for LD), in contrast to the wide range observed for intermediates of core metabolic pathways. (ii) Turnover rates of active pools were significantly higher ( $P < 0.01$ ) in SD plants, with the turnover

half-lives being 2.0 and 1.5 h for LD and SD, respectively (Supplemental Table S7).

### **Metabolite levels**

The relationship between metabolite levels and daylength was determined by measuring steady-state levels of amino acids, organic acids, and sucrose (Table 4). Leaves in SD had higher levels of alanine, aspartate, glutamine, glycine, and sucrose but lower levels of glycerate. Glycine showed the greatest difference, with levels 3.9 times higher in SD plants than in LD plants.

## **Discussion**

### **SD plants compensate for shorter days through multiple mechanisms**

Shorter days generally have a lower DLI and more time for dark respiration, reducing the carbon available for growth and accumulation of desired products. The reduced DLI could reduce the *rgr* by 44%, leading to a reduced DW of 15% of LD compared to the observed *rgr* in SD that was 84% of the LD *rgr*. Because plant growth can be exponential over some periods, the reduced SD *rgr* resulted in an observed final weight that was 51% of LD. The photosynthetic rate was 21% higher in SD than in LD (Table 1). The greater photosynthetic rate was associated with a greater stomatal conductance, such that the intercellular CO<sub>2</sub> concentration was the same in both treatments (Table 1). Mesophyll conductance was higher in SD plants, which was confirmed by the more negative  $\delta^{13}\text{C}$  (Table 1). There was a reduced rate of the G6P shunt in SD plants. This was observed in the INCA results shown in Fig. 3 and in the reduced  $R_L$  value seen in gas exchange data (Table 1). Again, for exponential growth, we determined the enhancement of photosynthetic rate would increase *rgr* from 0.175 (which would be expected if the *rgr* of SD plants were decreased from that of LD plants in proportion to the photoperiod or DLI) to 0.213, but this was still well short of the observed *rgr* of 0.263; therefore, even accounting for the increased rate of *A*, the yield is predicted to be 0.39 compared to the observed 0.79 (Table 2). This points to both increased light-use efficiency for carbon acquisition and increased allocation of fixed carbon to growth.

Some of the other adjustments seen in SD include changes in carbon partitioning. The higher rate of starch synthesis in SD plants (Fig. 3; Table 1) results in higher starch levels for the longer night. The greater investment in shoot relative to the root in SD plants (Fig. 1B) made more resources available for photosynthesis. Finally, the thinner leaves (Fig. 1C) allowed a greater leaf area for a given amount of resources invested per leaf area. This parameter, called the specific leaf area, is known to be associated with faster plant growth (Lambers et al. 2008; Weraduwage et al. 2015).

### **Natural abundance <sup>13</sup>C and <sup>15</sup>N levels**

In LD plants, carbon and nitrogen stable isotope content ( $\delta^{13}\text{C}$  and  $\delta^{15}\text{N}$ ) was higher (less negative for  $\delta^{13}\text{C}$ , and %

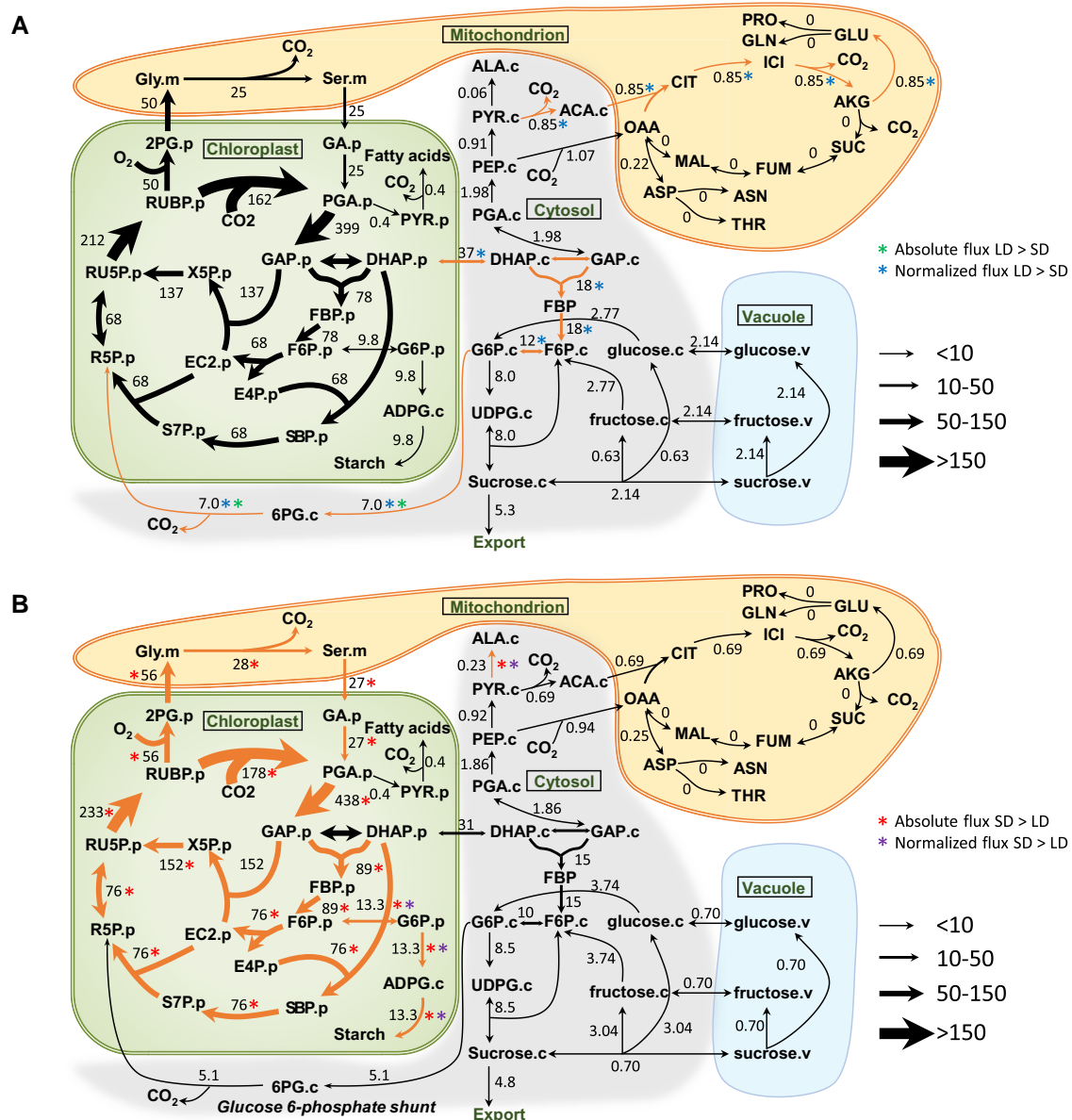


**Figure 3.** Central carbon metabolic fluxes in photosynthetic *C. sativa* leaves in LD and SD. **A)** Metabolic flux map in LD conditions. **B)** Metabolic flux map in SD conditions. Fluxes are shown as numbers and depicted by the variable width of arrows. Both absolute and normalized fluxes were compared by 95% confidence intervals between LD and SD (Supplemental Table S5). Absolute and normalized fluxes that are bigger in LD plants are marked by green asterisk (\*) and blue asterisk (\*), respectively. Absolute and normalized fluxes that are bigger in SD plants are marked by red asterisk (\*) and purple asterisk (\*), respectively. Flux differences are highlighted by orange arrows. Flux units are expressed as  $\mu\text{mol metabolite g}^{-1} \text{FW h}^{-1}$ . The model network is compartmentalized into cytosol (“c.”), chloroplast (“p.”), mitochondrion (“m.”), and vacuole (“v.”). 2PG, 2-phosphoglycolate; ACA, acetyl-CoA; AKG,  $\alpha$ -ketoglutarate; ALA, alanine; ASN, asparagine; ASP, aspartate; CIT, citrate; DHAP, dihydroxyacetone phosphate; EC2, transketolase-bound-2-carbon-fragment; FBP, fructose-1,6-bisphosphatase; FUM, fumarate; GA, glycerate; GLN, glutamine; GLY, glycine; ICI, isocitrate; MAL, malate; PEP, phosphoenolpyruvate; PYR, pyruvate; RU5P, ribulose-5-phosphate; RUBP, ribulose-1,5-bisphosphate; S7P, sedoheptulose-7-phosphate; SBP, sedoheptulose-1,7-bisphosphate; SER, serine; SUC, succinate; THR, threonine. All abbreviations are shown in Supplemental Table S10.

C and %N were lower (Supplemental Table S1). There was more discrimination against  $^{13}\text{CO}_2$  in SD plants. This indicates less diffusion resistance to  $\text{CO}_2$  uptake (Farquhar et al. 1982). Intercellular  $\text{CO}_2$  levels ( $C_i$ ) were the same in LD and SD leaves, so the best explanation is that mesophyll conductance for  $\text{CO}_2$  diffusion was greater in SD.

Mesophyll conductance becomes very difficult to obtain from fitting of  $A/C_i$  curves when it is very high. Although we could estimate mesophyll conductance in LD leaves, the fitting indicated a nonmeasurable mesophyll conductance in SD, consistent with the strong isotopic discrimination in SD leaves. This high mesophyll conductance could account for

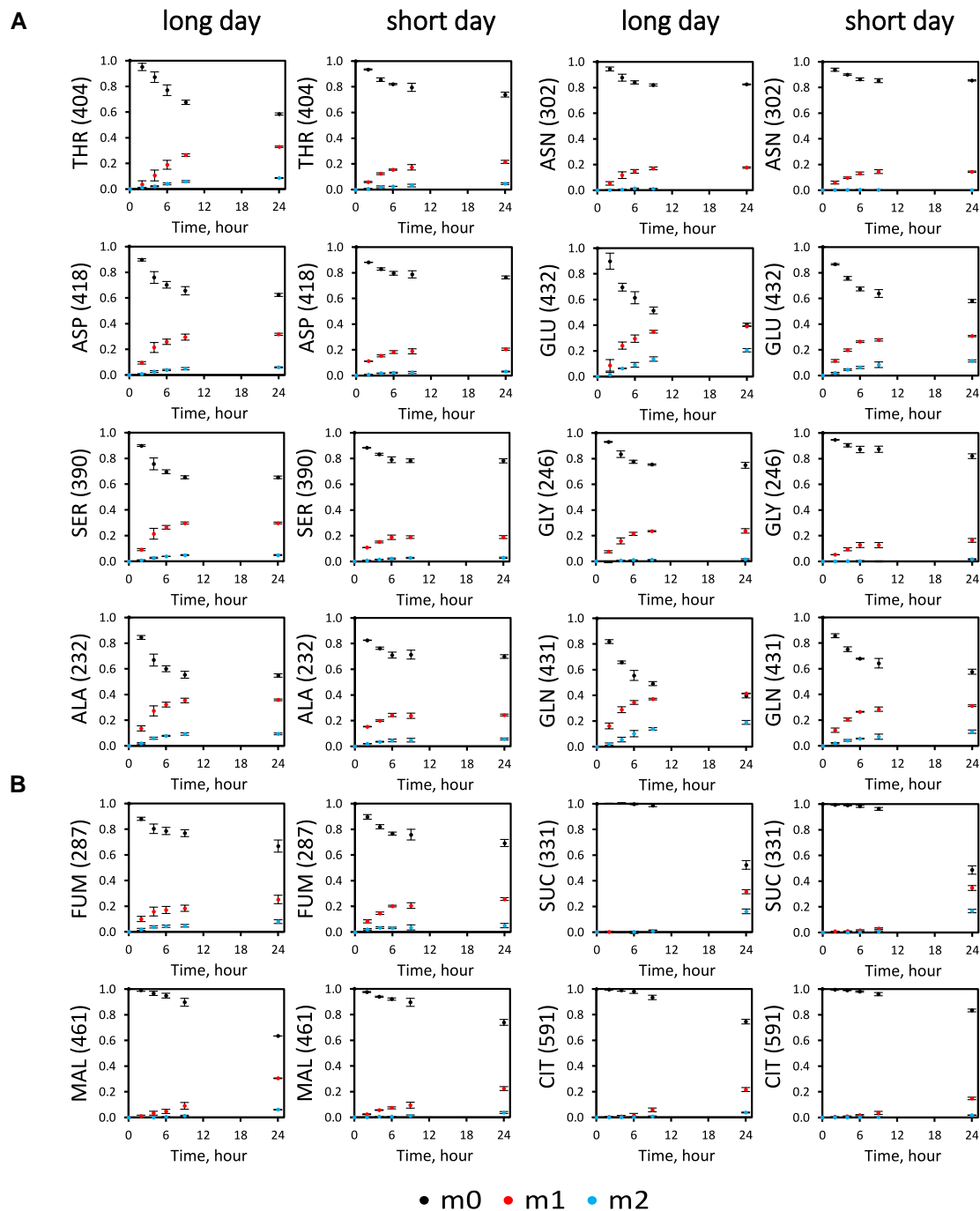


**Figure 4.**  $^2\text{H}_2\text{O}$ -labeling patterns for amino acids and organic acids in LD and SD from 0 to 24 h. **A)** Amino acid labeling patterns. **B)** Organic acid labeling patterns. MIDs are shown as points with error bars ( $n = 3$ ,  $\pm\text{sd}$ ). Nominal masses of M0 mass isotopologs are shown in parentheses. m0: unlabeled molecule with no isotopic atoms. m1: 1 atom isotopically labeled. m2: 2 atoms isotopically labeled. ALA, alanine; ASN, asparagine; ASP, aspartate; CIT, citrate; FUM, fumarate; GLN, glutamine; GLY, glycine; MAL, malate; SER, serine; SUC, succinate; THR, threonine. All abbreviations are shown in [Supplemental Table S10](#).

the  $2 \mu\text{mol m}^{-2} \text{s}^{-1}$  greater  $A$  not accounted for by reduced  $R_L$  in SD plants. The mechanism underlying the higher  $\delta^{15}\text{N}$  is less clear. This could be related to a change in nitrate reduction in leaves relative to other parts of the plant. This is indicated by the  $\alpha_5$  parameter that reflects nitrate reduction to balance nitrogen loss as serine leaves the system (Busch et al. 2018).

### Starch synthesis

Starch is the most abundant carbohydrate stored in plants (Lu et al. 2005). SD plants had a higher starch synthesis rate (Table 1), which agrees with many previous findings in other  $\text{C}_3$  species like *Arabidopsis* (Lu et al. 2005; Gibon et al. 2009; Sulpice et al. 2014), spinach (*Spinacia oleracea*)



**Table 4.** Metabolite pool sizes in LD and SD ( $n = 3$ ,  $\pm$  SD)

Metabolite	LD (nmol g <sup>-1</sup> FW)	SD (nmol g <sup>-1</sup> FW)
Alanine	87 ± 21	244 ± 64*
Asparagine	69 ± 19	129 ± 34
Aspartate	80 ± 14	172 ± 46*
Citrate	692 ± 98	900 ± 117
Fructose-6-phosphate	181 ± 26	205 ± 31
Fructose-16-bisphosphatase	14 ± 2	16 ± 3
Fumarate	819 ± 106	803 ± 96
Glucose 6-phosphate	186 ± 23	222 ± 16
Glyceraldehyde-3-phosphate/ dihydroxyacetone phosphate	60 ± 10	81 ± 18
Glutamate	224 ± 75	461 ± 145
Glutamine	39 ± 17	107 ± 29*
Glycerate	527 ± 107	219 ± 20*
Glycine	103 ± 35	404 ± 47*
Malate	1,071 ± 253	1,450 ± 205
Ribulose-5-phosphate/ xylulose-5-phosphate	43 ± 8	49 ± 9
3-Phosphoglyceric acid	128 ± 18	150 ± 21
Ribose-5-phosphate	20 ± 2	23 ± 2
Ribulose-15-bisphosphate	120 ± 24	130 ± 17
Sedoheptulose-7-phosphate	176 ± 23	208 ± 17
Serine	335 ± 77	470 ± 102
Succinate	257 ± 68	408 ± 92
Sucrose	433 ± 61	655 ± 133*
Threonine	59 ± 18	80 ± 21

Significant differences between LD and SD are marked with asterisks (Student's *t*-test,  $P < 0.05$ ).

(Robinson 1984; Baysdorfer and Robinson 1985), soybean (*Glycine max*) (Chatterton and Silvius 1979; Huber and Israel 1982), wheat (*Triticum aestivum*) (Sicher et al. 1982), barley (*Hordeum vulgare*) (Gordon et al. 1982), tobacco (*N. tabacum*) (Huber et al. 1984; Matt et al. 1998), tomato (*Solanum lycopersicum*) (Logendra and Janes 1992), potato (*Solanum tuberosum*) (Lorenzen and Ewing 1992), cucumber (*Cucumis sativus*) (Challa 1977), and pea (*Pisum sativum*) (Stitt et al. 1978) and C<sub>4</sub> species like maize (*Zea mays*) (Sicher et al. 1982) and sorghum (*Sorghum bicolor*) (Britz et al. 1987). The higher starch synthesis in SD may be related to a clock-based mechanism to satisfy the carbohydrate requirements in the longer night period (Mugford et al. 2014). The higher fraction of <sup>14</sup>CO<sub>2</sub> being incorporated into starch (Table 1) and higher normalized flux for starch synthesis (Fig. 3B; Supplemental Table S5) showed that the increased starch accumulation rate in SD plants is due to both higher photosynthetic rate and preferential incorporation of photosynthate into starch. This explains previously observed higher starch levels in SD plants at the end of the day. (Logendra et al. 1990; Yu et al. 2001; Zeeman et al. 2004).

### Sucrose biosynthesis

Sucrose is the major end product of photosynthesis in most plants (Baysdorfer and Robinson 1985), and its absolute synthesis rate was higher in SD plants (Fig. 2B; Supplemental Table S1). The reported effect of daylength on the rate of sucrose

synthesis is variable. The sucrose synthesis rate in SD plants can be higher (Sicher et al. 1982; Robinson 1984; Baysdorfer and Robinson 1985; Logendra et al. 1990), lower (Gordon et al. 1982; Huber and Israel 1982; Mugford et al. 2014), or the same (Chatterton and Silvius 1980) as LD plants. Baysdorfer and Robinson 1985 reported that when supplies of fixed carbon are limited, starch synthesis has priority over sucrose synthesis in SD plants. When sufficient fixed carbon is available, starch and sucrose synthesis rates can be increased simultaneously in SD plants. This agrees with our findings that short-term partitioning to sucrose was not increased in SD plants (Table 1), indicating that the higher sucrose synthesis rate in SD is mainly caused by a higher carbon assimilation rate.

### <sup>13</sup>C-labeling kinetics in central metabolism

Daylength increases the rate of labeling of photorespiratory intermediates except for glycerate (Fig. 2). The enrichments of 2PG, glycine, serine, and glycerate at 30 min were 94%, 87%, 81%, and 28% in LD plants and 90%, 30%, 73%, and 51% in SD plants (Supplemental Table S4). In addition, the daylength effect on <sup>13</sup>C incorporation into these intermediates showed inconsistent trends, with faster (glycerate), slower (glycine and serine), or similar rates of labeling (2PG) in SD plants compared to LD plants. This indicated that the different labeling kinetics of photorespiratory intermediates cannot be explained simply by different photorespiration rates. Therefore, the estimation of the photorespiration rate in leaves by <sup>13</sup>C MFA fitting the label in photorespiratory intermediates is not reliable. With information on labeling in different compartments and reactions involving these and additional intermediates, it may be possible to derive photorespiratory flux estimates reliably using the <sup>13</sup>C-labeling data in this system. We, therefore, believe that, currently, the measured  $v_o/v_c$  value from gas exchange measurements should, as described previously, be an input to the MFA model, not an output (Fu et al. 2022; Xu et al. 2022).

The labeling kinetics of the TCA cycle-derived amino acids are affected by daylength. The oxaloacetate (OAA)-derived amino acid aspartate showed higher <sup>13</sup>C enrichment in SD plants (Fig. 2B). Threonine, made from aspartate, also exhibited higher labeling in SD plants but at a slower rate than aspartate (Fig. 2B), indicating either a larger initial pool size or a slower turnover rate that may be associated with lower demand for threonine than aspartate in protein synthesis and amino transferase reactions.

### The effects of daylength on metabolic fluxes in plant central metabolism

The “G6P shunt” is believed to help stabilize photosynthesis during rapid, large changes in CO<sub>2</sub> fixation (Li et al. 2019; Preiser et al. 2019; Weise et al. 2019). Based on INST-MFA, the CO<sub>2</sub> released from the G6P shunt is the major contribution to R<sub>L</sub> in both LD (86%) and SD (85%) plants (Fig. 3; Supplemental Table S5), which further supports previous

findings that the G6P shunt is the primary source of  $R_L$  (Xu et al. 2021, 2022). The ~37% lower G6P shunt flux in SD plants also resulted in ~35% lower total amount of nonrespiratory  $\text{CO}_2$  release in SD plants (Supplemental Table S5).  $R_L$  holds much importance in comprehending carbon exchange across various scales, from individual leaves to the global scale (Rogers et al. 2014). As a process that results in carbon loss,  $R_L$  presents a potential target for enhancing photosynthetic efficiency and crop yields, which represents a major challenge in the field of plant biology (Grierson et al. 2011; Huber 2011; Kromdijk and Long 2016).

Alanine, as the product of transamination of pyruvate, showed a higher rate of synthesis (Fig. 3B) and exudation rates (Supplemental Table S6) but slower fractional  $^{13}\text{C}$  labeling in leaves of SD plants (Fig. 2B). This is due to a larger total alanine pool (Table 2), much of which may be in a less active pool, resulting in saturating  $^{13}\text{C}$ -labeling kinetics (Supplemental Fig. S1).

The rate of glutamate synthesis via TCA is lower in SD plants (Fig. 3; Supplemental Table S5). The lower rate of glutamate synthesis via the TCA cycle may be related to the higher rate of alanine synthesis, as these 2 pathways are competing for the same precursors, pyruvate, and nitrogen. In addition,  $^2\text{H}_2\text{O}$  labeling of glutamate at 24 h showed lower labeling in SD plants (Fig. 4), which may be related to a larger total glutamate pool (Table 2) in SD with a large portion of the less active pool as a result of saturating  $^{13}\text{C}$ -labeling kinetics (Supplemental Fig. S2B).

### $^2\text{H}$ -labeling kinetics in central metabolism

The practical challenges and expense of long-term  $^{13}\text{CO}_2$  labeling under relevant physiological conditions in planta make deuterated water an attractive alternative—one that has been used in studies of protein turnover and amino acid metabolism in plants for almost half a century (Mitra et al. 1976; Shaw et al. 1985; Yang et al. 2010). Because of the inhibitory effects of concentrated deuterium oxide on plant growth and development (Sacchi and Cocucci 1992), we used 30%  $^2\text{H}_2\text{O}$ , which has been used in previous studies and has been reported to have no substantial effect on the growth of *Arabidopsis* and maize at 40% and a modest impact on seedling growth at 30% over several days (Mitra et al. 1976; Jensen and Bandurski 1996; Yang et al. 2010).

The ability of a 2-pool model (Supplemental Table S7) to account for the labeling data supports the idea that vacuolar pools of these metabolites, which are known to exist in leaf cell vacuoles (Szecowka et al. 2013), exchange only slowly with the more rapidly metabolized pools in other organelles. Due to potentially large kinetic isotope effects on rates of reaction and equilibrium labeling levels at different molecular positions (Strassner et al. 2005), the absolute rates and pool sizes cannot currently be deduced from the  $^2\text{H}$ -labeling data. However, relative rates and pool sizes in SD and LD plants can be quantitatively deduced.

While total amino acid levels are higher in SD plants (Table 1), the active pools represent a smaller proportion

of the total in SD plants, showing that the larger metabolite levels in SD plants represent a larger increase in vacuolar pools than in active pools. Despite their higher total levels, turnover rates for the active pools of amino acids were  $1.3 \pm 0.2$ -fold higher in SD plants (Supplemental Table S7). This ratio is close to the ratio of photosynthetic rates and is in keeping with the higher fluxes across central metabolism in the leaves of SD plants.

### The effects of daylength on metabolite pool sizes and subcellular compartmentation

The intracellular pool sizes of alanine, aspartate, glutamine, glycerate, glycine, and sucrose are affected by daylength (Table 2). Interestingly, measured changes in pool sizes of some metabolites were inversely associated with their  $^{13}\text{C}$ - and  $^2\text{H}$ -labeling patterns and indicated the presence of metabolically inactive pools that limited the proportion of each metabolite that became labeled over the time course (30 min for  $^{13}\text{C}$  and 24 h for  $^2\text{H}$  labeling). For example, glycine reached an isotopic steady state with only 30% of the pool labeled with  $^{13}\text{C}$  in SD (Fig. 2B), suggesting the existence of pools in multiple compartments, with large inactive pools that cannot be labeled within the studied labeling time. The lower  $^2\text{H}$  incorporation (Fig. 4) and higher pool size (Table 1) of glycine in SD plants also reflected subcellular features. This pattern is consistent with several other metabolites. Combining information on pool sizes, subcellular compartmentation, export rates, and labeling kinetics over the diel cycle allows a full picture of carbon and nitrogen dynamics to emerge.

Subcellular compartmentalization is a ubiquitous challenge for isotopic labeling studies because of the presence of metabolically active pools of the same metabolite in different organelles (Allen et al. 2007; Moreira et al. 2019). Direct subcellular metabolite measurements can be made by non-aqueous fractionation (Gerhardt and Heldt 1984; Arrivault et al. 2014), although this has not yet been combined with labeling for  $^{13}\text{C}$  MFA. Obtaining compartmentation information on labeling and pool sizes of these metabolites would allow metabolic models of cellular metabolism to define flux patterns with greater detail and confidence.

### Conclusions

In this study, the effects of daylength on plant growth, photosynthesis, carbon partitioning, and the overall influence of plant primary metabolism were comprehensively studied in *C. sativa* grown in LD and SD conditions. We found SD plants compensated for the shorter photoperiod through several adaptations: greater mesophyll conductance to  $\text{CO}_2$  diffusion and reduced  $R_L$ , resulting in shoot investment with higher photosynthetic rates, reduced rates of the G6P shunt, and greater partitioning of sugars to starch sustaining C availability in the longer night.  $^2\text{H}$ -labeling kinetics suggested that vacuolar pools of metabolites exchange slowly with other cellular compartments. Despite higher total amino acid levels in

SD plants, the active pools had higher turnover rates and were associated with higher fluxes across central metabolism. These findings provide insights into adjustments of metabolic and compartmentation in response to daylength and have potential implications for ecological adaptation, as well as pointing to potential future approaches for improving crop yield in plants grown under varying latitudes and seasons.

## Materials and methods

### Plant growth, gas exchange, and $^{13}\text{CO}_2$ labeling

False flax (*C. sativa*) plants (ecotype var. Calena) were grown under LD (16-h light/8-h-dark) and SD (9-h-light/15-h-dark) photoperiods at a light intensity of  $500 \mu\text{mol m}^{-2} \text{s}^{-1}$ , temperatures of  $22^\circ\text{C}$ , and relative humidity of 50%. Calculated DLI was  $16.2 \text{ mol d}^{-1}$  for the SD treatment and  $28.8 \text{ mol d}^{-1}$  for the LD treatment. Plants were grown in a mixture of potting medium consisting of 70% peat moss, 21% perlite, and 9% vermiculite (by volume) (Suremix; Michigan Grower Products Inc., Galesburg, MI, USA) and were fertilized with 1/4 strength Hoagland's solution (Hoagland and Arnon 1950). Gas exchange and  $^{13}\text{CO}_2$ -labeling experiments were as described previously (Xu et al. 2022) with slight modifications. Fully expanded leaves on 4-wk-old plants were used for  $^{13}\text{CO}_2$ -labeling experiments. A LI-COR 6800 portable photosynthesis system (LI-COR Biosciences, Lincoln, NE, USA) was used to measure  $\text{CO}_2$  assimilation rate, stomatal conductance, and other photosynthetic parameters. The reference ( $\text{CO}_2$ ) was set to 400 ppm, light intensity was  $500 \mu\text{mol m}^{-2} \text{s}^{-1}$ , temperature was  $22^\circ\text{C}$ , and water vapor pressure difference (VPD) was 1.0 kPa. The  $^{13}\text{CO}_2$  labeling was initiated after a period of 20 to 30 min to reach a stable photosynthetic state. The  $\text{CO}_2$  source was switched to  $^{13}\text{CO}_2$  with all other parameters held constant, and a pseudosteady-state metabolism was assumed during the labeling period. Gases were mixed with mass flow controllers (Alicat Scientific, Tucson, AZ, USA) controlled by a custom-programmed Raspberry Pi touchscreen monitor (Raspberry Pi Foundation, code available upon request). Labeled leaf samples were collected at time points of 0, 0.5, 1, 2, 3, 5, 7, 10, 15, and 30 min. Liquid nitrogen was directly sprayed on the leaf surface via a customized fast-quenching labeling system, as described previously (Xu et al. 2021). Sampling was conducted between 9:00 AM and 4:00 PM, with time points for sampling selected randomly. One leaf was sampled as a single biological replicate, and 3 biological replicates were collected for each time point. A total of 60 leaves, gathered from 40 plants, were used. The frozen leaf sample was stored at  $-80^\circ\text{C}$ .

### Deuterium oxide labeling

The deuterium oxide labeling method was developed and performed on 4-wk-old *C. sativa* plants. Plants were subjected to a 3-d period of water deprivation prior to the labeling experiment. On the day of labeling, at approximately

8:00 AM, each plant was watered with about 500 mL of 30% (v/v) deuterium oxide ( $\text{D}_2\text{O}$ , 99.9%) (Cambridge Isotope Laboratories, USA) diluted in 1/4 strength Hoagland's solution. Three biological replicates of fully expanded leaves were collected from random plants at 0, 2, 4, 6, 9, and 24 h after watering, frozen in liquid nitrogen, and stored at  $-80^\circ\text{C}$  before extraction. A total of 36 leaves, gathered from 12 plants, were used. All the sampling time points were during the light period to avoid diel effects.

### Growth rate of shoot and root, leaf fresh weight, and leaf chlorophyll content

The DWs of both shoot and root systems were measured in 14-, 17-, 21-, 24-, and 28-d-old *C. sativa* plants with 6 replicates per time point. A total of 60 plants were used. The samples were harvested by taking the entire plant out of the soil, washing off any loose soil, separating the roots and shoots, and drying at  $60^\circ\text{C}$  for 15 d until the weight was stable.  $r_{\text{grs}}$  were calculated from the plant weight time course data (see Supplemental Method S1 and Tables S2 and S8). The fresh weight per leaf area and chlorophyll content were measured using a  $1\text{-cm}^2$  leaf punch from 5 randomly selected mature leaves on different plants. Chlorophyll content was measured using the method described by Arnon (1949), with slight modifications. The concentration of leaf chlorophyll a, chlorophyll b, and total chlorophyll (Chl a, Chl b, and Chl t) was measured on fresh leaf samples taken from 5 randomly selected plants. After chopping into small pieces, each leaf sample was extracted by incubation overnight in acetone:water (80:20 v/v) at  $4^\circ\text{C}$ . Samples were then centrifuged ( $12,000 \times g$ ) for 5 min. The supernatant's absorbance was measured at wavelengths of 645 and 663 nm on a spectrophotometer (Hitachi U2000, Japan) and converted to chlorophyll amounts as described in (Arnon 1949). A total of 10 leaves, gathered from 5 plants, were used. The statistical analysis was performed using Student's *t*-test.

### A/C<sub>i</sub> curve measurements and parameter calculation

A/C<sub>i</sub> curves were measured with a LI-COR 6800 portable photosynthesis system (LI-COR Biosciences, Lincoln, NE, USA) with light intensity of  $500 \mu\text{mol photon m}^{-2} \text{s}^{-1}$ , leaf temperature of  $22^\circ\text{C}$ , and VPD of 1.0 kPa. The sequence of reference  $\text{CO}_2$  partial pressures was 5, 6, 8, 10, 12, 15, 18, 20, 25, 30, 35, 40, 50, 60, 80, 100, 120, and 150 Pa (Supplemental Fig. S4). A total of 8 leaves, gathered from 4 plants, were used. Photosynthetic parameters including the maximum Rubisco carboxylation rate ( $V_{\text{cmax}}$ ), the maximum attained rate of electron transport ( $J$ ), respiration in the light ( $R_L$ ), mesophyll conductance to  $\text{CO}_2$  transfer ( $g_m$ ), the rate of triose phosphate utilization (TPU), and the proportion of carbon exported from photorespiration as glycine ( $\alpha_G$ ) or serine ( $\alpha_S$ ) were estimated from the A/C<sub>i</sub> curves using the R-script, which was described in detail previously (Sharkey 2016; Gregory et al. 2021) and is available at <https://github.com/poales/msuRACiFit> (Supplemental Table S1).



### Carbon and nitrogen natural abundance isotope analysis ( $\delta^{13}\text{C}$ , $\delta^{15}\text{N}$ , %C, and %N)

Four replicates, each containing 10 randomly selected fully expanded leaves from different plants, were collected and dried at 60 °C for 15 d. A total of 10 leaves, gathered from 5 plants, were used. The dried samples were then ground into a fine powder, encapsulated in tin cups, and submitted to the University of Arkansas stable isotope laboratory (<https://isotope.uark.edu/>) for carbon and nitrogen isotope analysis, as described in detail in [Supplemental Method S2](#).

### Metabolite extraction and mass spectrometry analyses

Metabolites were extracted from rapidly frozen tissues as described previously ([Xu et al. 2021](#)). Known concentrations of internal standards (including nor-Leucine, 98 atom %  $^{15}\text{N}$  and 98 atom %  $^{13}\text{C}$  free amino acid mixture, D-[UL- $^{13}\text{C}_6$ ] fructose 1,6-bisphosphate, and [UL- $^{13}\text{C}_{12}$ ] sucrose) were spiked into the unlabeled samples before extraction for pool size quantification. Metabolites were analyzed by mass spectrometry as previously described ([Xu et al. 2021, 2022](#)) with slight modification. MS parameters for transitions of measured metabolites in multiple reaction monitoring (MRM) with LC-MS/MS and selected ion monitoring (SIM) with GC-MS are shown in [Supplemental Table S9](#).

### IPC-MS/MS analysis

Phosphorylated intermediates in the CBC cycle were analyzed by ion-pair chromatography–tandem mass spectrometry (IPC-MS/MS) by an ACQUITY UPLC pump system (Waters, Milford, MA, USA) coupled with Waters XEVO TQ-S UPLC/MS/MS (Waters, Milford, MA, USA). Metabolites were separated by a 2.1 × 50 mm ACQUITY UPLC BEH C18 Column (Waters, Milford, MA, USA) at 40 °C. A multistep gradient was applied with mobile phase A (10 mM tributylamine in 5% [v/v] methanol) and mobile phase B (methanol): 0 to 1 min, 95% to 85% A; 1 to 6 min, 65% to 40% A; 6 to 7 min, 40% to 0% A; 7 to 8 min, 0% A; and 8 to 9 min, 100% A, at a flow rate of 0.3 mL min<sup>-1</sup>. The source temperature was 120 °C, and the desolvation temperature was 350 °C. Nitrogen was used as a sheath and auxiliary gas, and collision gas (argon) was set to 1.1 mTorr. Gas flow for the desolvation and cone was set to 800 and 50 L/h, respectively. The scan time was 0.1 ms.

### AEC-MS/MS analysis

Nucleotide sugars and additional phosphorylated intermediates (i.e. 2PG and phosphoenolpyruvate) were analyzed by anion exchange chromatography–tandem mass spectrometry (AEC-MS/MS) by an ACQUITY UPLC pump system (Waters, Milford, MA, USA) coupled with a Xevo ACQUITY TQ Triple Quadrupole Detector (Waters, Milford, MA, USA). Metabolites were separated by an IonPac AS11 analytical column (2 × 250 mm, Dionex) equipped with an IonPac

Guard Column AG11 (2 × 50 mm, Dionex) at a flow rate of 0.35 mL min<sup>-1</sup>. A multistep gradient was applied with mobile phase A (0.5 mM KOH) and mobile phase B (75 mM KOH): 0 to 2 min, 100% A; 2 to 4 min, 100% to 93% A; 4 to 13 min, 93% to 60% A; 13 to 15 min, 0% A; and 15 to 17 min, 100% A. The KOH concentration was suppressed by a postcolumn anion self-regenerating suppressor (Dionex ADRS 600, Thermo Scientific, Waltham, MA, USA), with a current of 50 mA and flow rate of 3.5 mL min<sup>-1</sup>. An IonPac ATC-3 Anion Trap Column (4 × 35 mm), conditioned with 2 M KOH, was used to remove contaminant ions from KOH solvents.

### GC-MS analysis

Amino acids, organic acids, and sugars were analyzed by GC-MS by an Agilent 7890 GC system (Agilent, Santa Clara, CA, USA) coupled to an Agilent 5975C inert XL Mass Selective Detector (Agilent, Santa Clara, CA, USA). Samples were first derivatized by methoxyamine hydrochloride dissolved in dry pyridine at room temperature overnight. Amino acids and organic acids were silylated to trimethylsilyl (TBDMS) derivatives by adding *N*-(tert-butyldimethylsilyl)-*N*-methyltrifluoroacetamide with 1% (w/v) tert-butyldimethylchlorosilane and incubated at 60 °C overnight. Sugars were silylated to trimethylsilyl (TMS) derivatives by adding *N*,*O*-bis(trimethylsilyl)trifluoroacetamide with 1% (w/v) trimethylchlorosilane and incubated at 60 °C overnight. Metabolites were separated by an Agilent VF5ms GC column (Agilent, Santa Clara, CA, USA). The inlet temperature and MS transfer line temperature were set at 230 °C and 300 °C, respectively. The oven temperature was initially held at 40 °C for 1 min and then raised at 40 °C/min to 80 °C, 10 °C/min to 240 °C, and 20 °C/min until reaching 320 °C, which was maintained for 5 min. Electron ionization (EI) was at 70 eV, and the mass scan range was 50 to 600 amu.

### Analysis of mass spectrometry data

Data analysis for quantifying MIDs and pool sizes was described previously ([Xu et al. 2022](#)) with slight modifications. Data from LC-MS/MS were acquired with MassLynx 4.0 (Agilent, Santa Clara, CA, USA). Data from GC-MS were acquired from Agilent GC/MSD ChemStation (Agilent, Santa Clara, CA, USA). Metabolites were identified by retention time and mass-to-charge ratio (*m/z*) in comparison with authentic standards. Both LC-MS and GC-MS data were converted to MassLynx format and processed with QuanLynx software for peak detection and quantification. MIDs for each metabolite in which  $^{13}\text{C}$  or  $^2\text{H}$  atoms are incorporated can be calculated using the following equation:

$$\text{MID}_n = \frac{M_n}{\sum_{j=0}^i M_j}$$

*M<sub>n</sub>* represents the isotopolog abundance for each metabolite.

Experimentally measured  $^{13}\text{C}$  and  $^2\text{H}$  MIDs were corrected for natural abundance using IsoCor ([Millard et al. 2019](#)) and FluxFix ([Trefely et al. 2016](#)) software and are shown in [Supplemental Tables S3 and S7](#).



### Isotopolog network, flux determination, and assessment of flux precision

INST-MFA was performed to estimate metabolic fluxes using the Isotopomer Network Compartmental Analysis software package (INCA2.1, <http://mfa.vueinnovations.com>, Vanderbilt University; Young 2014) with the metabolic network model established previously (Xu et al. 2022). A list of the reactions and abbreviations is provided in Supplemental Table S10. The stoichiometry of reactions and atom transitions for each reaction are shown in Supplemental Table S11. Metabolite MIDs, CO<sub>2</sub> assimilation rate, starch synthesis rate,  $v_o/v_c$ , and vascular exudate composition were provided as inputs to the model. Goodness of fit was measured by the SSRs by quantifying the total difference between measured and simulated kinetics, which was minimized to obtain flux values for the best-fitting models for LD and SD plants (Supplemental Table S5). The parameter continuation method (Young 2014) was used to estimate the 95% confidence intervals for both absolute fluxes and normalized fluxes of best-fit models (Supplemental Table S5). The computationally intensive confidence interval determination was performed in parallel using a SLURM job scheduler to distribute jobs to hundreds of computer nodes within a high-performance computing cluster at the Institute for Cyber-Enabled Research at Michigan State University (<https://icer.msu.edu/>).

### Starch synthesis rate and fractions of starch and sucrose

Starch levels were measured using a total starch (AA/AMG) test kit (Megazyme, Bray, Wicklow, Ireland) as described earlier (Xu et al. 2021). Partitioning of recently fixed carbon to starch and sucrose was measured via <sup>14</sup>C-labeling experiments during steady-state photosynthetic assimilation as described previously (Sharkey et al. 1985) with slight modifications. <sup>14</sup>CO<sub>2</sub> gas was mixed with CO<sub>2</sub>-free air using mass flow controllers (Alicat Scientific, Tucson AZ, USA) and flowed through the sample port on the back of a head of a LI-6800 (LI-COR Biosciences, Lincoln, NE, USA). The reference CO<sub>2</sub> was set to 400 ppm, light intensity was 500 μmol m<sup>-2</sup> s<sup>-1</sup>, temperature was 22 °C, and humidity for VPD was 1.0 kPa. Each leaf was pulsed with <sup>14</sup>CO<sub>2</sub> for 10 min with a CO<sub>2</sub> concentration of 400 μL L<sup>-1</sup>. The <sup>14</sup>C-labeled leaf sample was cut and frozen immediately in liquid nitrogen, followed by a measurement of its fresh weight. Frozen samples were stored at –80 °C prior to extraction. The sampling period ranged from 9:00 AM to 4:00 PM, with random selection of time points for sampling. One leaf was sampled at each time point, and 6 biological replicates were collected for each time point. Each leaf sample was extracted with 0.5-mL formic acid solution (formic acid/ethanol 4:75, v/v). The suspension was centrifuged at 12,000 × g at 4 °C for 10 min. Half of the supernatant was counted for radioactivity (total soluble fraction) using a 1450 Microbeta Trilux scintillation counter (PerkinElmer, Waltham, MA, USA). The other half of the supernatant was passed through a cation exchange resin (Dowex 50WX8 H+ form) column (Sigma-Aldrich, St. Louis,

MO, USA), followed by an anion exchange resin (Dowex 1X8 Cl- form) column (Sigma-Aldrich, St. Louis, MO, USA). The initial 1-mL flow through was discarded, and the following five 1-mL flow throughs were collected separately and counted for radioactivity (neutral soluble fraction). The ionic fraction was calculated as the difference between the total soluble fraction and the neutral soluble fraction. The pellet was washed twice with 850-μL water and twice with 850-μL 80% ethanol (v/v) and then resuspended in 0.5 mL of 0.2 M KOH. Starch in the pellet was gelatinized at 95 °C for 30 min, and then 90 μL of 1 M acetic acid was added to bring the pH to 5. Starch was digested with 50 U alpha-amylase (Sigma-Aldrich, St. Louis, MO, USA) and 6.5 U amyloglucosidase (Sigma-Aldrich, St. Louis, MO, USA) for 2 d at room temperature. The supernatant was collected after centrifugation and subjected to radioactivity counting. The proportion of counts in the starch and neutral soluble fractions (mostly sucrose) relative to total counts were calculated.

### Vascular exudate composition measurement

The export flux of carbon from leaves to other parts of the plant was estimated as previously described (Xu et al. 2021) by measuring the vascular exudate composition, expressed as the ratio between sucrose and the major amino acids glutamate, aspartate, alanine, glycine, and serine. Fresh leaves were cut at the base and placed in a sealed pressure bomb chamber. Pressurized gas was slowly added to the chamber until the exudates were forced out of the vasculature and visible at the cut end of the petiole protruding from the chamber. Exudates were collected from 3 randomly selected mature leaves of different plants. Sucrose and amino acids in the exudates were analyzed using GC-MS as described above.

### Acknowledgments

The authors appreciate the assistance of Dr. Berkley Walker (MSU) for helpful discussions; Ms. Emily Pawlowski and Mr. Cody Keilen (MSU Growth Chamber Facility) for growth chamber and plant maintenance; Dr. Daniel Jones, Dr. Lijun Chen, and Dr. Casey Johnny (MSU Mass Spectrometry and Metabolomics Core Facility) for assistance of mass spectrometry methods; Dr. Erik Pollock (University of Arkansas Stable Isotope Lab) for analyzing carbon and nitrogen isotope composition; MSU Institute for Cyber-Enabled Research for providing high-performance computing cluster and services; and Dr. Jamey Young for making INCA accessible.

### Author contributions

Y.S.-H. and Y.X. conceived the study; Y.S.-H., T.D.S., and Y.X. designed the experiments. A.A.K. performed growth measurements. Y.X. performed the <sup>13</sup>C- and <sup>2</sup>H- labeling experiments, metabolite analyses, and MFAs and analyzed the results. S.E.W. advised and assisted Y.X. with the <sup>14</sup>CO<sub>2</sub> pulse-chase experiment. X.F. advised and assisted Y.X. with the A/Ci measurements, which were analyzed by T.D.S. Y.X. wrote the

manuscript with contributions from T.D.S. and Y.S.-H. Y.S.-H. serves as the author responsible for contact and ensures communication.

## Supplemental data

The following materials are available in the online version of this article.

**Supplemental Figure S1.** Transient  $^{13}\text{C}$  labeling of glycine, serine, aspartate, threonine, alanine, sucrose fructosyl moiety, and sucrose glucosyl moiety in LD and SD.

**Supplemental Figure S2.** Transient  $^{13}\text{C}$  labeling of metabolites that showed similar patterns in LD and SD plants.

**Supplemental Figure S3.** Analysis of  $^2\text{H}_2\text{O}$ -labeling time course results.

**Supplemental Figure S4.**  $A/C_i$  curve measurement for LD A) and SD B).

**Supplemental Table S1.** Effect of daylength on parameters of photosynthesis,  $A/C_i$  analysis, and leaf properties.

**Supplemental Table S2.** Calculation of  $rgr$  based on observed data (orange cells) or predicted DWs from adjusted  $rgr$ .

**Supplemental Table S3.** MIDs of measured metabolites in  $^{13}\text{C}$  labeling experiments.

**Supplemental Table S4.**  $^{13}\text{C}$  enrichment of measured metabolites in  $^{13}\text{C}$  labeling experiments.

**Supplemental Table S5.** Estimated flux values and 95% confidence intervals by parameter continuation.

**Supplemental Table S6.** Vascular exudates composition and output fluxes.

**Supplemental Table S7.** MIDs of measured metabolites in  $^2\text{H}_2\text{O}$ -labeling experiments.

**Supplemental Table S8.** The DW of the shoot and root systems from 14 to 28 days ( $n = 6, \pm\text{sd}$ ).

**Supplemental Table S9.** Parameters for transitions of measured metabolites in LC-MS/MS and GC-MS.

**Supplemental Table S10.** Abbreviations for metabolites and reactions.

**Supplemental Table S11.** The stoichiometry of reactions and atom transitions for each reaction of LD and SD models.

**Supplemental Method S1.** Effect of reduced DLI on plant growth.

**Supplemental Method S2.** Carbon and nitrogen natural abundance isotope analysis ( $\delta^{13}\text{C}$ ,  $\delta^{15}\text{N}$ , %C, and %N).

## Funding

This work was supported by the Division of Chemical Sciences, Geosciences and Biosciences, Office of Basic Energy Sciences of the US Department of Energy, grants DE-FOA-0001650 and DEFG02-91ER20021. T.D.S. receives partial salary support from MSU AgBioResearch.

*Conflict of interest statement.* None declared.

## Data availability

The authors confirm that the data supporting the findings of this study are available within the article and its [Supplemental materials](#).

## References

- Adebiyi AO, Jazmin LJ, Young JD.**  $^{13}\text{C}$  flux analysis of cyanobacterial metabolism. *Photosynth Res.* 2015;**126**(1):19–32. <https://doi.org/10.1007/s11120-014-0045-1>
- Allen DK, Shachar-Hill Y, Ohlrogge JB.** Compartment-specific labeling information in  $^{13}\text{C}$  metabolic flux analysis of plants. *Phytochemistry* 2007;**68**(16–18):2197–2210. <https://doi.org/10.1016/j.phytochem.2007.04.010>
- Arnon DI.** Copper enzymes in isolated chloroplasts. Polyphenoloxidase in *Beta vulgaris*. *Plant Physiol.* 1949;**24**(1):1–15. <https://doi.org/10.1104/pp.24.1.1>
- Arrivault S, Guenther M, Florian A, Encke B, Feil R, Vosloh D, Lunn JE, Sulpice R, Fernie AR, Stitt M.** Dissecting the subcellular compartmentation of proteins and metabolites in *Arabidopsis* leaves using non-aqueous fractionation. *Mol Cell Proteomics.* 2014;**13**(9):2246–2259. <https://doi.org/10.1074/mcp.M114.038190>
- Arrivault S, Guenther M, Ivakov A, Feil R, Vosloh D, Van Dongen JT, Sulpice R, Stitt M.** Use of reverse-phase liquid chromatography, linked to tandem mass spectrometry, to profile the Calvin cycle and other metabolic intermediates in *Arabidopsis* rosettes at different carbon dioxide concentrations. *Plant J.* 2009;**59**(5):826–839. <https://doi.org/10.1111/j.1365-313X.2009.03902.x>
- Basler G, Fernie AR, Nikoloski Z.** Advances in metabolic flux analysis toward genome-scale profiling of higher organisms. *Biosci Rep.* 2018;**38**(6):BSR20170224. <https://doi.org/10.1042/BSR20170224>
- Baysdorfer C, Robinson JM.** Sucrose and starch synthesis in spinach plants grown under long and short photosynthetic periods. *Plant Physiol.* 1985;**79**(3):838–842. <https://doi.org/10.1104/pp.79.3.838>
- Bernardo A, Howard-Hildige R, O'Connell A, Nichol R, Ryan J, Rice B, Roche E, Leahy JJ.** *Camelina* oil as a fuel for diesel transport engines. *Ind Crops Prod.* 2003;**17**(3):191–197. [https://doi.org/10.1016/S0926-6690\(02\)00098-5](https://doi.org/10.1016/S0926-6690(02)00098-5)
- Berti M, Gesch R, Eynck C, Anderson J, Cermak S.** *Camelina* uses, genetics, genomics, production, and management. *Ind Crops Prod.* 2016;**94**:690–710. <https://doi.org/10.1016/j.indcrop.2016.09.034>
- Britz SJ, Hungerford WE, Lee DR.** Rhythms during extended dark periods determine rates of net photosynthesis and accumulation of starch and soluble sugars in subsequent light periods in leaves of *Sorghum*. *Planta* 1987;**171**(3):339–345. <https://doi.org/10.1007/BF00398679>
- Budin JT, Breene WM, Putnam DH.** Some compositional properties of *Camelina* (*Camelina sativa* L. Crantz) seeds and oils. *J Am Oil Chem Soc.* 1995;**72**(3):309–315. <https://doi.org/10.1007/BF02541088>
- Busch FA, Sage RF, Farquhar GD.** Plants increase  $\text{CO}_2$  uptake by assimilating nitrogen via the photorespiratory pathway. *Nat plants.* 2018;**4**(1):46–54. <https://doi.org/10.1038/s41477-017-0065-x>
- Casal JJ, Fankhauser C, Coupland G, Blázquez MA.** Signalling for developmental plasticity. *Trends Plant Sci.* 2004;**9**(6):309–314. <https://doi.org/10.1016/j.tplants.2004.04.007>
- Challa H.** An analysis of the diurnal course of growth, carbon dioxide exchange and carbohydrate reserve content of cucumber. Wageningen 1976: Centre for Agricultural Publishing and Documentation; 1977.
- Chatterton NJ, Silviu JE.** Photosynthate partitioning into starch in soybean leaves: I. Effects of photoperiod versus photosynthetic period duration. *Plant Physiol.* 1979;**64**(5):749–753. <https://doi.org/10.1104/pp.64.5.749>
- Chatterton NJ, Silviu JE.** Acclimation of photosynthate partitioning and photosynthetic rates to changes in length of the daily photosynthetic period. *Ann Bot.* 1980;**46**(6):739–745. <https://doi.org/10.1093/oxfordjournals.aob.a085971>

- Cheah YE, Young JD.** Isotopically nonstationary metabolic flux analysis (INST-MFA): putting theory into practice. *Curr Opin Biotechnol.* 2018;**54**:80–87. <https://doi.org/10.1016/j.copbio.2018.02.013>
- Chu KL, Koley S, Jenkins LM, Bailey SR, Kambhampati S, Foley K, Arp JJ, Morley SA, Czymmek KJ, Bates PD.** Metabolic flux analysis of the non-transitory starch tradeoff for lipid production in mature tobacco leaves. *Metab Eng.* 2022;**69**:231–248. <https://doi.org/10.1016/j.ymben.2021.12.003>
- Ciubota-Rosie C, Ruiz JR, Ramos MJ, Pérez Á.** Biodiesel from *Camelina sativa*: a comprehensive characterisation. *Fuel* 2013;**105**:572–577. <https://doi.org/10.1016/j.fuel.2012.09.062>
- Clark TJ, Guo L, Morgan J, Schwender J.** Modeling plant metabolism: from network reconstruction to mechanistic models. *Annu Rev Plant Biol.* 2020;**71**(1):303–326. <https://doi.org/10.1146/annurev-arplant-050718-100221>
- Farquhar GD, O'Leary MH, Berry JA.** On the relationship between carbon isotope discrimination and the intercellular carbon dioxide concentration in leaves. *Funct Plant Biol.* 1982;**9**(2):121–137. <https://doi.org/10.1071/PP9820121>
- Fu X, Gregory LM, Weise SE, Walker BJ.** Integrated flux and pool size analysis in plant central metabolism reveals unique roles of glycine and serine during photorespiration. *Nat Plants.* 2022;**9**(1):169–178. <https://doi.org/10.1038/s41477-022-01294-9>
- Gerhardt R, Heldt HW.** Measurement of subcellular metabolite levels in leaves by fractionation of freeze-stopped material in nonaqueous media. *Plant Physiol.* 1984;**75**(3):542–547. <https://doi.org/10.1104/pp.75.3.542>
- Gibon Y, Pyl ET, Sulpice R, Lunn JE, Höhne M, Günther M, Stitt M.** Adjustment of growth, starch turnover, protein content and central metabolism to a decrease of the carbon supply when *Arabidopsis* is grown in very short photoperiods. *Plant Cell Environ.* 2009;**32**(7):859–874. <https://doi.org/10.1111/j.1365-3040.2009.01965.x>
- Gomez-Cano F, Carey L, Lucas K, García Navarrete T, Mukundi E, Lundback S, Schnell D, Grotewold E.** Camregbase: a gene regulation database for the biofuel crop, *Camelina sativa*. *Database.* 2020;**2020**. <https://doi.org/10.1093/database/baaa075>
- Gordon AJ, Ryle GJA, Mitchell DF, Powell CE.** The dynamics of carbon supply from leaves of barley plants grown in long or short days. *J Exp Bot.* 1982;**33**(2):241–250. <https://doi.org/10.1093/jxb/33.2.241>
- Gregory LM, McClain AM, Kramer DM, Pardo JD, Smith KE, Tessmer OL, Walker BJ, Ziccardi LG, Sharkey TD.** The triose phosphate utilization limitation of photosynthetic rate: out of global models but important for leaf models. *Plant Cell Environ.* 2021;**44**(10):3223–3226. <https://doi.org/10.1111/pce.14153>
- Grierson CS, Barnes SR, Chase MW, Clarke M, Grierson D, Edwards KJ, Jellis GJ, Jones JD, Knapp S, Oldroyd G, et al.** One hundred important questions facing plant science research. *New Phytol.* 2011;**192**(1):6–12. <https://doi.org/10.1111/j.1469-8137.2011.03859.x>
- Guo W, Sheng J, Feng X.** <sup>13</sup>C-metabolic flux analysis: an accurate approach to demystify microbial metabolism for biochemical production. *Bioengineering* 2015;**3**(1):3. <https://doi.org/10.3390/bioengineering3010003>
- Hasunuma T, Harada K, Miyazawa SI, Kondo A, Fukusaki E, Miyake C.** Metabolic turnover analysis by a combination of in vivo <sup>13</sup>C-labelling from <sup>13</sup>CO<sub>2</sub> and metabolic profiling with CE-MS/MS reveals rate-limiting steps of the C<sub>3</sub> photosynthetic pathway in *Nicotiana tabacum* leaves. *J Exp Bot.* 2010;**61**(4):1041–1051. <https://doi.org/10.1093/jxb/erp374>
- Hoagland DR, Arnon DI.** The water-culture method for growing plants without soil. *Circ Calif Agric Exp Stn.* 1950;**347**:13143–13151.
- Huber SC.** Grand challenges in plant physiology: the underpinning of translational research. *Front Plant Sci.* 2011;**2**:48. <https://doi.org/10.3389/fpls.2011.00048>
- Huber SC, Israel DW.** Biochemical basis for partitioning of photosynthetically fixed carbon between starch and sucrose in soybean (*Glycine max* Merr.) Leaves. *Plant Physiol.* 1982;**69**(3):691–696. <https://doi.org/10.1104/pp.69.3.691>
- Huber SC, Rufty TW, Kerr PS.** Effect of photoperiod on photosynthate partitioning and diurnal rhythms in sucrose phosphate synthase activity in leaves of soybean (*Glycine max* L. [Merr.]) and tobacco (*Nicotiana tabacum* L.). *Plant Physiol.* 1984;**75**(4):1080–1084. <https://doi.org/10.1104/pp.75.4.1080>
- Jackson SD.** Plant responses to photoperiod. *New Phytol.* 2009;**181**(3):517–531. <https://doi.org/10.1111/j.1469-8137.2008.02681.x>
- Jensen PJ, Bandurski RS.** Incorporation of deuterium into indole-3-acetic acid and tryptophan in *Zea mays* seedlings grown on 30% deuterium oxide. *J Plant Physiol.* 1996;**147**(6):697–702. [https://doi.org/10.1016/S0176-1617\(11\)81480-X](https://doi.org/10.1016/S0176-1617(11)81480-X)
- Kromdijk J, Long SP.** One crop breeding cycle from starvation? How engineering crop photosynthesis for rising CO<sub>2</sub> and temperature could be one important route to alleviation. *Proc R Soc B Biol Sci.* 2016;**283**(1826):20152578. <https://doi.org/10.1098/rspb.2015.2578>
- Kruger NJ, Ratcliffe RG.** Fluxes through plant metabolic networks: measurements, predictions, insights and challenges. *Biochem J.* 2015;**465**(1):27–38. <https://doi.org/10.1042/BJ20140984>
- Kruger NJ, Ratcliffe RG.** Whither metabolic flux analysis in plants? *J Exp Bot.* 2021;**72**(22):7653–7657. <https://doi.org/10.1093/jxb/erab389>
- Kurasiak-Popowska D, Graczyk M, Przybylska-Balcerek A, Stuper-Szablewska K.** Influence of variety and weather conditions on fatty acid composition of winter and spring *Camelina sativa* varieties in Poland. *Eur Food Res Technol.* 2021;**247**(2):465–473. <https://doi.org/10.1007/s00217-020-03639-0>
- Kurasiak-Popowska D, Stuper-Szablewska K, Nawracała J.** *Camelina* oil as a natural source of carotenoids for the cosmetic industry. *Przem Chem.* 2017;**96**:2077–2080. <https://doi.org/10.15199/62.2017.10.8>
- Lambers H, Chapin FS, Pons TL.** Plant physiological ecology. New York: Springer; 2008.
- Li J, Weraduwege SM, Preiser AL, Tietz S, Weise SE, Strand DD, Froehlich JE, Kramer DM, Hu J, Sharkey TD.** A cytosolic bypass and G6P shunt in plants lacking peroxisomal hydroxypyruvate reductase. *Plant Physiol.* 2019;**180**(2):783–792. <https://doi.org/10.1104/pp.19.00256>
- Li T, Pang N, He L, Xu Y, Fu X, Tang Y, Shachar-Hill Y, Chen S.** Re-programming glucose catabolism in the microalga *Chlorella sorokiniana* under light condition. *Biomolecules* 2022;**12**(7):939. <https://doi.org/10.3390/biom12070939>
- Logendra S, Janes HW.** Light duration effects on carbon partitioning and translocation in tomato. *Sci Hortic (Amsterdam).* 1992;**52**(1–2):19–25. [https://doi.org/10.1016/0304-4238\(92\)90004-V](https://doi.org/10.1016/0304-4238(92)90004-V)
- Logendra S, Putman JD, Janes HW.** The influence of light period on carbon partitioning, translocation and growth in tomato. *Sci Hortic (Amsterdam).* 1990;**42**(1–2):75–83. [https://doi.org/10.1016/0304-4238\(90\)90149-9](https://doi.org/10.1016/0304-4238(90)90149-9)
- Lorenzen JH, Ewing EE.** Starch accumulation in leaves of potato (*Solanum tuberosum* L.) during the first 18 days of photoperiod treatment. *Ann Bot.* 1992;**69**(6):481–485. <https://doi.org/10.1093/oxfordjournals.aob.a088375>
- Lu Y, Gehan JP, Sharkey TD.** Daylength and circadian effects on starch degradation and maltose metabolism. *Plant Physiol.* 2005;**138**(4):2280–2291. <https://doi.org/10.1104/pp.105.061903>
- Ma F, Jazmin LJ, Young JD, Allen DK.** Isotopically nonstationary <sup>13</sup>C flux analysis of changes in *Arabidopsis thaliana* leaf metabolism due to high light acclimation. *Proc Natl Acad Sci.* 2014;**111**(47):16967–16972. <https://doi.org/10.1073/pnas.1319485111>
- Matt P, Schurr U, Klein D, Krapp A, Stitt M.** Growth of tobacco in short-day conditions leads to high starch, low sugars, altered diurnal changes in the *Nia* transcript and low nitrate reductase activity, and inhibition of amino acid synthesis. *Planta* 1998;**207**(1):27–41. <https://doi.org/10.1007/s004250050452>
- Millard P, Delépine B, Guionnet M, Heuillet M, Bellvert F, Létisse F.** Isocor: isotope correction for high-resolution MS labeling



- experiments. *Bioinformatics* 2019;**35**(21):4484–4487. <https://doi.org/10.1093/bioinformatics/btz209>
- Mitra R, Burton J, Varner JE.** Deuterium oxide as a tool for the study of amino acid metabolism. *Anal Biochem.* 1976;**70**(1):1–17. [https://doi.org/10.1016/S0003-2697\(76\)80042-5](https://doi.org/10.1016/S0003-2697(76)80042-5)
- Moreira TB, Lima JM, Coca GC, Williams TCR.** Insights into the spatial and temporal organisation of plant metabolism from network flux analysis. *Theor Exp Plant Physiol.* 2019;**31**(1):215–226. <https://doi.org/10.1007/s40626-018-0132-3>
- Moser BR, Vaughn SF.** Evaluation of alkyl esters from *Camelina sativa* oil as biodiesel and as blend components in ultra low-sulfur diesel fuel. *Bioresour Technol.* 2010;**101**(2):646–653. <https://doi.org/10.1016/j.biortech.2009.08.054>
- Mugford ST, Fernandez O, Brinton J, Flis A, Krohn N, Encke B, Feil R, Sulpice R, Lunn JE, Stitt M, et al.** Regulatory properties of ADP glucose pyrophosphorylase are required for adjustment of leaf starch synthesis in different photoperiods. *Plant Physiol.* 2014;**166**(4):1733–1747. <https://doi.org/10.1104/pp.114.247759>
- Preiser AL, Fisher N, Banerjee A, Sharkey TD.** Plastidic glucose-6-phosphate dehydrogenases are regulated to maintain activity in the light. *Biochem J.* 2019;**476**(10):1539–1551. <https://doi.org/10.1042/BCJ20190234>
- Righini D, Zanetti F, Martínez-Force E, Mandrioli M, Toschi TG, Monti A.** Shifting sowing of *Camelina* from spring to autumn enhances the oil quality for bio-based applications in response to temperature and seed carbon stock. *Ind Crops Prod.* 2019;**137**:66–73. <https://doi.org/10.1016/j.indcrop.2019.05.009>
- Robinson JM.** Photosynthetic carbon metabolism in leaves and isolated chloroplasts from spinach plants grown under short and intermediate photosynthetic periods. *Plant Physiol.* 1984;**75**(2):397–409. <https://doi.org/10.1104/pp.75.2.397>
- Rogers A, Medlyn BE, Dukes JS.** Improving representation of photosynthesis in Earth System Models. *New Phytol.* 2014;**204**(1):12–14. <https://doi.org/10.1111/nph.12972>
- Sacchi GA, Cocucci M.** Effects of deuterium oxide on growth, proton extrusion, potassium influx, and in vitro plasma membrane activities in maize root segments. *Plant Physiol.* 1992;**100**(4):1962–1967. <https://doi.org/10.1104/pp.100.4.1962>
- Schwender J, Ohlrogge J, Shachar-Hill Y.** Understanding flux in plant metabolic networks. *Curr Opin Plant Biol.* 2004;**7**(3):309–317. <https://doi.org/10.1016/j.pbi.2004.03.016>
- Sharkey TD.** What gas exchange data can tell us about photosynthesis. *Plant Cell Environ.* 2016;**39**(6):1161–1163. <https://doi.org/10.1111/pce.12641>
- Sharkey TD, Berry JA, Raschke K.** Starch and sucrose synthesis in *Phaseolus vulgaris* as affected by light, CO<sub>2</sub>, and abscisic acid. *Plant Physiol.* 1985;**77**(3):617–620. <https://doi.org/10.1104/pp.77.3.617>
- Shastri AA, Morgan JA.** A transient isotopic labeling methodology for <sup>13</sup>C metabolic flux analysis of photoautotrophic microorganisms. *Phytochemistry* 2007;**68**(16–18):2302–2312. <https://doi.org/10.1016/j.phytochem.2007.03.042>
- Shaw NM, Parsley KR, Davies DD.** Amino-acid biosynthesis in the cotyledons of *Sinapis alba* L. in darkness and far-red light studied by deuterium labelling and mass spectrometry. *Planta* 1985;**165**(4):561–568. <https://doi.org/10.1007/BF00398104>
- Shonnard DR, Williams L, Kalnes TN.** *Camelina*-derived jet fuel and diesel: sustainable advanced biofuels. *Environ Prog Sustain Energy.* 2010;**29**(3):382–392. <https://doi.org/10.1002/ep.10461>
- Sicher RC, Harris WG, Kremer DF, Chatterton NJ.** Effects of shortened day length upon translocation and starch accumulation by maize, wheat, and pangola grass leaves. *Can J Bot.* 1982;**60**(8):1304–1309. <https://doi.org/10.1139/b82-166>
- Stephanopoulos GN, Aristidou AA, Nielsen J.** *Metabolic engineering: principles and methodologies* 1998 .
- Stitt M, Bulpin P V, Ap Rees T.** Pathway of starch breakdown in photosynthetic tissues of *Pisum sativum*. *BBA—Gen Subj.* 1978;**544**(1):200–214. [https://doi.org/10.1016/0304-4165\(78\)90223-4](https://doi.org/10.1016/0304-4165(78)90223-4)
- Strassner T, Kohen A, Limbach H, Kohen A, Limbach H.** In: **Kohen A, Limbach H,** editors. *Isotope effects in chemistry and biology.* CRC Press; 2005. p. 281–301.
- Sulpice R, Flis A, Ivakov AA, Apelt F, Krohn N, Encke B, Abel C, Feil R, Lunn JE, Stitt M.** *Arabidopsis* coordinates the diurnal regulation of carbon allocation and growth across a wide range of photoperiods. *Mol Plant.* 2014;**7**(1):137–155. <https://doi.org/10.1093/mp/sst127>
- Szewocka M, Heise R, Tohge T, Nunes-Nesi A, Vosloh D, Huege J, Feil R, Lunn J, Nikoloski Z, Stitt M, et al.** Metabolic fluxes in an illuminated *Arabidopsis* rosette. *Plant Cell* 2013;**25**(2):694–714. <https://doi.org/10.1105/tpc.112.106989>
- Trefely S, Ashwell P, Snyder NW.** FluxFix: automatic isotopologue normalization for metabolic tracer analysis. *BMC Bioinformatics* 2016;**17**(1):1–8. <https://doi.org/10.1186/s12859-016-1360-7>
- Ver Sagun J, Yadav UP, Alonso AP.** Progress in understanding and improving oil content and quality in seeds. *Front Plant Sci.* 2023;**14**:1116894. <https://doi.org/10.3389/fpls.2023.1116894>
- Weise SE, Liu T, Childs KL, Preiser AL, Katulski HM, Perrin-Porzondek C, Sharkey TD.** Transcriptional regulation of the glucose-6-phosphate/phosphate translocator 2 is related to carbon exchange across the chloroplast envelope. *Front Plant Sci.* 2019;**10**:827. <https://doi.org/10.3389/fpls.2019.00827>
- Weraduwege SM, Chen J, Anozie FC, Morales A, Weise SE, Sharkey TD.** The relationship between leaf area growth and biomass accumulation in *Arabidopsis thaliana*. *Front Plant Sci.* 2015;**6**:167. <https://doi.org/10.3389/fpls.2015.00167>
- Xu Y, Fu X, Sharkey TD, Shachar-Hill Y, Walker BJ.** The metabolic origins of non-photorespiratory CO<sub>2</sub> release during photosynthesis: a metabolic flux analysis. *Plant Physiol.* 2021;**186**(1):297–314. <https://doi.org/10.1093/plphys/kiab076>
- Xu Y, Wieloch T, Kaste JAM, Shachar-Hill Y, Sharkey TD.** Reimport of carbon from cytosolic and vacuolar sugar pools into the Calvin–Benson cycle explains photosynthesis labeling anomalies. *Proc Natl Acad Sci.* 2022;**119**(11):e2121531119. <https://doi.org/10.1073/pnas.2121531119>
- Yang XY, Chen WP, Rendahl AK, Hegeman AD, Gray WM, Cohen JD.** Measuring the turnover rates of *Arabidopsis* proteins using deuterium oxide: an auxin signaling case study. *Plant J.* 2010;**63**(4):680–695. <https://doi.org/10.1111/j.1365-313X.2010.04266.x>
- Young JD.** INCA: a computational platform for isotopically non-stationary metabolic flux analysis. *Bioinformatics* 2014;**30**(9):1333–1335. <https://doi.org/10.1093/bioinformatics/btu015>
- Young JD, Shastri AA, Stephanopoulos G, Morgan JA.** Mapping photoautotrophic metabolism with isotopically nonstationary <sup>13</sup>C flux analysis. *Metab Eng.* 2011;**13**(6):656–665. <https://doi.org/10.1016/j.ymben.2011.08.002>
- Yu TS, Kofler H, Häusler RE, Hille D, Flügge UI, Zeeman SC, Smith AM, Kossmann J, Lloyd J, Ritte G, et al.** The *Arabidopsis* *sex1* mutant is defective in the R1 protein, a general regulator of starch degradation in plants, and not in the chloroplast hexose transporter. *Plant Cell* 2001;**13**(8):1907–1918. <https://doi.org/10.1105/TPC.010091>
- Zeeman SC, Smith SM, Smith AM.** The breakdown of starch in leaves. *New Phytol.* 2004;**163**(2):247–261. <https://doi.org/10.1111/j.1469-8137.2004.01101.x>
- Zubr J.** Qualitative variation of *Camelina sativa* seed from different locations. *Ind Crops Prod.* 2003;**17**(3):161–169. [https://doi.org/10.1016/S0926-6690\(02\)00091-2](https://doi.org/10.1016/S0926-6690(02)00091-2)